Quaternary Research

doi:10.1017/qua.2018.133

Cosmogenic Cl-36 surface exposure dating of late Quaternary glacial events in the Cordillera de Talamanca, Costa Rica

Rebecca Potter[a], Yingkui Li[a]*, Sally P. Horn[a], Kenneth H. Orvis[a]

[a]Department of Geography, University of Tennessee, Knoxville, Tennessee 37996, USA
*Corresponding author e-mail address: yli32@utk.edu

(Received April 12, 2018; Accepted October 15, 2018)

Abstract

Geomorphic evidence of past glaciation, such as U-shaped valleys, aretes, glacial lakes, and moraines, is preserved in the highland surrounding Cerro Chirripó in the Cordillera de Talamanca, Costa Rica. Previous work to establish a glacial chronology has focused on relative age dating of moraines and on radiocarbon dating of basal lake sediments to infer the timing of deglaciation. We used cosmogenic ^{36}Cl surface exposure dating to constrain the ages of moraines within two formerly glaciated valleys, the Morrenas and Talari valleys. Forty-nine boulder samples were processed and measured from four moraine complexes in the Morrenas Valley and two moraine complexes in the Talari Valley. The exposure ages of these samples indicate a major glacial event occurred in this area from ~25 to 23 ka, broadly synchronous with the global last glacial maximum. Our results also indicate periods of glacial retreats and standstills from the deglacial period to the Early Holocene (~16–10 ka) before the complete disappearance of glaciers in this highland. These findings provide important insights into the glacial chronology and paleoclimate of tropical America.

Keywords: Late Quaternary; Glaciation; Costa Rica; Cosmogenic ^{36}Cl surface exposure dating; Tropics

INTRODUCTION

The role of the tropics in climate change has garnered significant attention in recent decades (e.g., Cane, 1998; Seltzer, 2001; Chiang, 2009; Jomelli et al., 2014). However, debate still exists on the nature of climate change in the tropics and on the connections between drivers of climate variations in the tropics and those in the middle to high latitudes (e.g., Seltzer, 2001; Farber et al., 2005; Smith et al., 2005, 2008; Licciardi et al., 2009; Jomelli et al., 2014). Glaciers in tropical mountains are highly sensitive to climate change (Kaser and Osmaston, 2002; Benn et al., 2005). Thus, constraining the timing and extent of past glacial fluctuations in tropical mountains is of key importance for understanding tropical paleoclimate trends and their forcing mechanisms. However, it has been difficult to constrain ages of the landforms left behind by past glaciers, so exploiting the climate information they contain has been difficult or impossible. The development of cosmogenic nuclide surface exposure dating (e.g., Gosse and Phillips, 2001; Li and Harbor, 2009) provides a unique opportunity to date glacial landforms and thereby address important paleoclimate issues, including whether glacial advances were synchronous or asynchronous between the tropics and middle/high latitudes (e.g., Gillespie and Molnar, 1995; Smith et al., 2005, 2008; Schaefer et al., 2006, 2009; Clark et al., 2009; Licciardi et al., 2009; Smith and Rodbell, 2010; Jomelli et al., 2014).

With their great combined latitudinal extent, the mountain ranges of tropical America—from the central Mexican volcanoes through Central America and southward through the Andes to Bolivia—are ideal places to reconstruct past glacier fluctuations in the tropics and to examine the climatic linkages between the tropics and middle/high latitudes (Hastenrath, 2009). To date, most studies using cosmogenic nuclides to constrain glacial chronologies are from Southern Hemisphere sites in the Peruvian and Bolivian Andes (mainly ^{10}Be), such as the Junin Plain (Smith et al., 2005, 2008), the Cordillera Blanca (Farber et al., 2005; Glasser et al., 2009; Smith and Rodbell, 2010), the Cordillera Vicabamba (Licciardi et al., 2009), the Cordillera Huayhuash (Hall et al., 2009), the Nevado Coropuna (Bromley et al., 2009), and the Cordillera Real (Smith et al., 2011). In the northern neotropics, cosmogenic nuclide ages are available from the

Cite this article: Potter, R., Li, Y., Horn, S. P., Orvis, K. H. 2019. Cosmogenic Cl-36 surface exposure dating of late Quaternary glacial events in the Cordillera de Talamanca, Costa Rica. *Quaternary Research* 92, 216–231.

central Mexican volcanoes (^{36}Cl; Vázquez-Selem and Heine, 2004) and the Merida Andes, Venezuela (^{10}Be; Wesnousky et al., 2012; Carcaillet et al., 2013; Angel et al., 2016). Glacial features have been documented and mapped in the Sierra de los Cuchumatanes, Guatemala, most thoroughly by Roy and Lachniet (2010), but no radiometric ages are available (Lachniet and Roy, 2011). In Costa Rica, dating has focused on basal organic sediments in glacial lakes within the cirques (Orvis and Horn, 2000), which provide the minimum ages of the last deglaciation. Knowledge of glacial chronologies in the northern neotropics is thus incomplete, hindering efforts to understand the role of the tropics in triggering, transmitting, and amplifying interhemispheric climate signals.

In the work reported here, we constrained the timing of glacial events around Cerro Chirripó in the Cordillera de Talamanca, Costa Rica, using cosmogenic ^{36}Cl surface exposure dating. This work establishes a glacial chronology in this key area of Central America that can be used to test whether glacial events in this area were synchronous with those documented in the tropical Andes and Central Mexico. The findings from this research provide important insights into paleoclimate and environmental changes in tropical America.

STUDY AREA

Our study area is the small upland massif surrounding Cerro Chirripó (3819 meters above sea level [m asl]; 9°29.05'N, 83°29.32'W) on the northwestern end of the Cordillera de Talamanca in Costa Rica (Fig. 1). Cerro Chirripó, the highest point on the massif and in all of Costa Rica, is a glacial horn and a popular hiking destination near the center of the remote Chirripó National Park. The peaks and upland valleys of the Chirripó massif extend above the regional treeline and are covered by neotropical páramo vegetation dominated by the miniature bamboo *Chusquea subtessellata,* other grasses, and shrubs (Kappelle and Horn, 2005, 2016). The Cerro Páramo meteorologic station (3466 m asl; 9°33.60'N, 83° 45.18'W), about 30 km west of Cerro Chirripó in the páramo of the Buenavista massif, recorded a mean annual precipitation of 2581 mm and a mean annual temperature of 8.5°C between 1971 and 2000 (Lane et al., 2011). Snow has not been officially recorded in Costa Rica, though the Swiss geographer and botanist Henri Pittier reported a mixture of rain and snow, with no accumulation, on Cerro Buenavista in January 1897 (Herrera, 2005; Castillo-Muñoz, 2010).

The Chirripó and Buenavista massifs preserve important records of Pleistocene tropical climate in glacial landforms (Hastenrath, 1973; Orvis and Horn, 2000; Lachniet and Seltzer, 2002; Lachniet, 2004, 2007; Lachniet and Vazquéz-Selem, 2005; Castillo-Muñoz, 2010) and lake sediments (Horn, 1990, 1993; Lane et al., 2011; Lane and Horn, 2013), as well as in highland bogs (Martin, 1964; Islebe and Hooghiemstra, 1997) and paleosols (Driese et al., 2007) beyond the ice limit. Glacial features near Cerro Chirripó, where they are most extensive, were first reported by Weyl (1956a, 1956b). Hastenrath (1973) identified specific moraine complexes and speculated on ages but was unable to find suitable material in moraines for dating. Bergoeing (1977) interpreted glacial geomorphology from aerial photographs, Barquero and Ellenberg (1983, 1986) mapped glacial features from fieldwork and aerial photograph analyses, and Wunsch et al. (1999) mapped and interpreted glacial features along with rock types from fieldwork. Horn (1990) inferred the timing of deglaciation from radiocarbon dating of basal organic and transitional sediments in the largest lake in the Morrenas Valley. Orvis and Horn (2000) obtained sediment cores and radiocarbon dates from additional lakes, mapped moraines, and reconstructed equilibrium line altitudes (ELAs) and past ice extents corresponding to these moraines in the Morrenas Valley. Lachniet and Seltzer (2002) and Lachniet and Vázquez-Selem (2005) investigated and mapped glacial features across the massif, reconstructed ELAs, and examined the weathering of boulders on moraines attributed to two different glacial stages. Orvis and Horn (2000) and Lachniet and Seltzer (2002) both proposed that an ice cap covered the Chirripó massif during the late Pleistocene; Lachniet and Seltzer (2002) also presented evidence on past ice extent on two other high peaks in the Cordillera de Talamanca—Cerro Buenavista (also called Cerro de la Muerte), along the Inter-American Highway crossing to the west of Cerro Chirripó, and Cerro Kamuk near the border with Panama.

Some uncertainty exists as to which climate factors most affected glacial advance and retreat in this area. Hastenrath (2009) suggested that the ELA for mountain glaciers in the inner humid tropics may be more sensitive to temperature variation than to precipitation variation. Lachniet and Seltzer (2002) conjectured that ELA temperature depressions in Costa Rica during the late Quaternary might be associated with a steeper lapse rate resulting from drier climate conditions produced by an equatorward restriction or weakening of the Intertropical Convergence Zone. From the reconstruction of ELAs and past glacial extents, Orvis and Horn (2000) speculated that both temperature (cold) and precipitation (drier or wetter) conditions influenced late Quaternary glacial fluctuations in the Cordillera de Talamanca.

This study focuses on two valleys next to Cerro Chirripó: the Morrenas and Talari Valleys. Bedrock consists of dacitic volcanic rocks, sedimentary rocks, and crystalline granitoid intrusives (Wunsch et al., 1999). The Morrenas Valley is a formerly glaciated, north/northwest-facing valley adjacent to the Chirripó headwall. Within the cirque, glacial lakes and moraines create a hummocky terrain surrounded by valley walls with limited vegetation growth on top of bedrock (Horn et al., 2005). The sizes of the lakes vary, but the largest measures 5.6 ha and 8.3 m deep (Horn et al., 2005). The gradient of the valley floor steepens downvalley from the cirque. The Talari Valley faces southwest. Its cirque also has a hummocky terrain (but without glacial lakes), and the valley gradient steepens downvalley from the cirque. On the northwest side of the upper Talari Valley, freeze-thaw processes have produced solifluction terraces in the ablation till mantling the slope (Lachniet and Seltzer, 2002).

Orvis and Horn (2000) mapped four moraine complexes in the Morrenas Valley: Chirripó IV (oldest), III, II, and I

https://doi.org/10.1017/qua.2018.133 Published online by Cambridge University Press

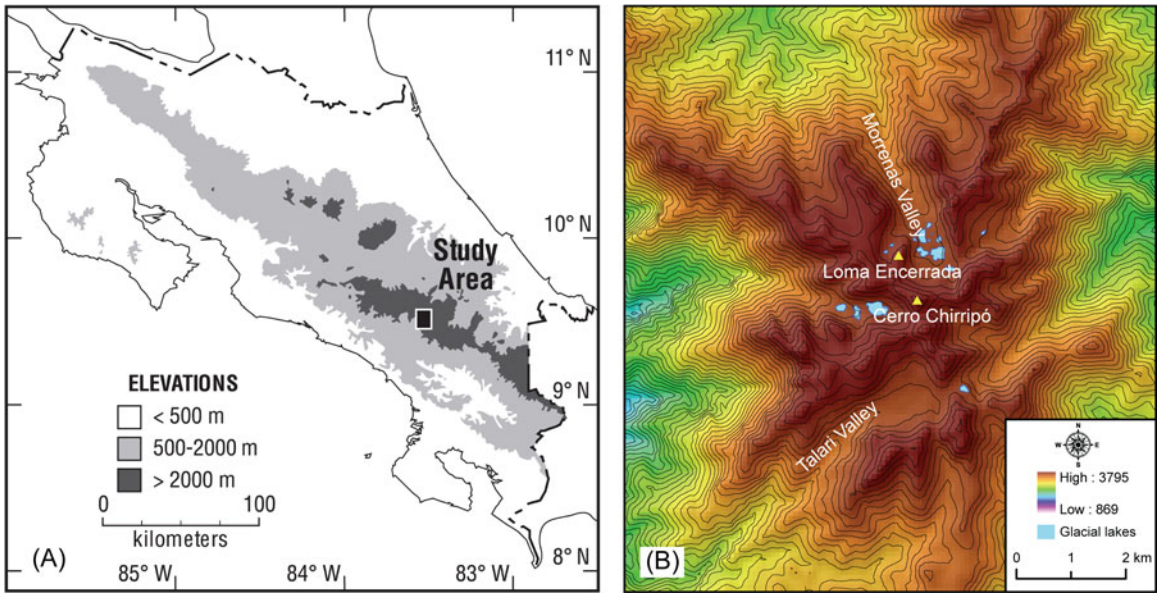

Figure 1. (color online) (A) Map of Costa Rica showing location of Chirripó massif in the Cordillera de Talamanca. (B) Shaded relief of the study area derived using the 90 m Shuttle Radar Topography Mission digital elevation model (http://srtm.csi.cgiar.org, last accessed on July 20, 2018). The Morrenas Valley is located on the north flank and the Talari Valley on the southwest flank of the massif. The contour interval is 50 m.

(youngest) (Fig. 2). The Chirripó IV moraine (M-4 in Fig. 2) corresponds to the oldest and largest glacial advance in this valley, and it is ~3.2 km downvalley (reaches to 3310 m asl) from the Chirripó headwall. The Chirripó III moraine (M-3 in Fig. 2) is ~0.9 km upvalley from the Chirripó IV moraine (2.3 km from Chirripó headwall). The Chirripó II moraine (M-2 in Fig. 2) is ~0.8 km upvalley from the Chirripó III moraine (1.6 km from Chirripó headwall). The Chirripó I moraine complex (M-1 in Fig. 2) is within the cirque and includes a set of moraines that surround glacial lakes. We carried out cosmogenic nuclide surface exposure dating of moraines from all four complexes.

We also investigated two moraines in the Talari Valley. The lower moraine (T-II in Fig. 2) is ~2.6 km downvalley (reaches to 3349 m asl) from the valley headwall. The upper moraine (T-I in Fig. 2; reaches to 3357 m asl) is very close to and just about 0.3 km upvalley from the lower moraine. Lachniet and Seltzer (2002) examined moraines and other glacial features throughout the Chirripó massif and identified three moraine groups in the Morrenas and Talari Valleys (Talamanca, Chirripó, and Talari), corresponding to the Chirripó IV–II moraines of Orvis and Horn (2000). The two moraines we studied in the Talari Valley (T-II and T-I) correspond to the Talamanca and Chirripó moraines, respectively, described by Lachniet and Seltzer (2002).

Radiocarbon ages from lake sediment cores in the Morrenas Valley indicated that the last glacial advance could correspond in time to the Younger Dryas, with this advance followed by complete deglaciation sometime after 12.4 ka cal BP but before 9.7 ka cal BP (Orvis and Horn, 2000). These radiocarbon dates on basal lake sediment correspond to the youngest moraine complex (Chirripó I) identified by Orvis and Horn (2000) and were the only dates available to the researchers. Like Hastenrath (1973), Orvis and Horn (2000) were unable to secure organic material from moraines for radiocarbon dating. Based on studies in Mexico and South America, the researchers suggested a polystage interpretation in which the Chirripó II moraine complex was associated with Marine Oxygen Isotope Stage (MIS) 2, and they tentatively correlated Chirripó III with MIS 4 and Chirripó IV with MIS 6. Lachniet and Seltzer (2002) measured pedestal heights of quartz veins on boulders and bedrock associated with their Chirripó stage (equivalent to Orvis and Horn's Chirripó III) and Talamanca stage (Chirripó IV), and from this work, they inferred that these two stages might be only a few thousand years different in age. They suggested that their Talari (Chirripó II) moraines could represent features formed during small advances or recessions during the Chirripó (Chirripó III) phase, as interpreted by Hastenrath (1973). Wunsch et al. (1999), in a study not available to Orvis and Horn (2000) or Lachniet and Seltzer (2002), classified all moraines except the oldest set as recessional, describing them as a series of "backstepping terminal and lateral moraines" formed by "oscillations during the backmelting stage" (Wunsch et al. 1999, p. 194). However, until the study we describe here, no absolute dating results were available from moraines in the Chirripó highlands to test these competing ideas.

METHODS

Sample collection, processing, and measurement

On three expeditions to the Chirripó highlands in 1998, 2000, and 2001, we collected 56 boulder samples from moraines for

https://doi.org/10.1017/qua.2018.133 Published online by Cambridge University Press

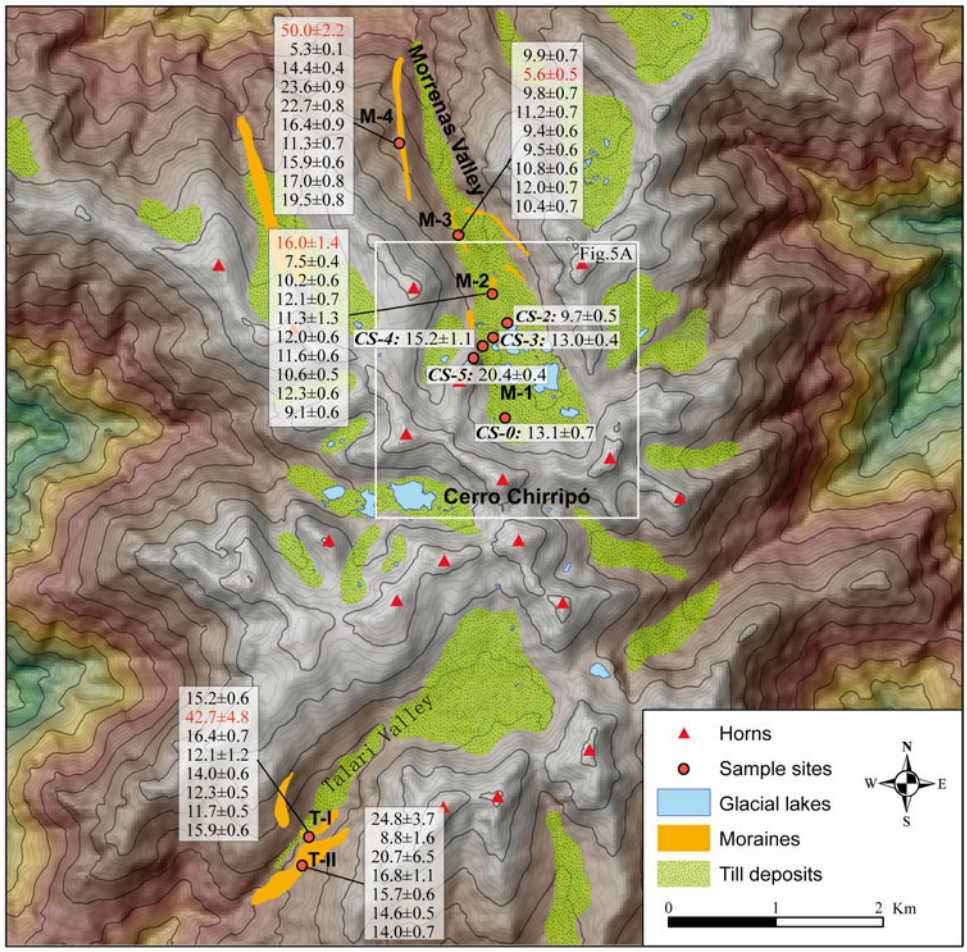

Figure 2. Geomorphological map of the study area, including moraines, till deposits, glacial lakes, and the sample sites in the Morrenas and Talari Valleys. Red dots show the sample sites for ^{36}Cl surface exposure dating. Samples CS-0 to CS-5 were collected from the cirque of the Morrenas Valley in 1998. Each dot on other moraines (M-4, M-3, and M-2 in the Morrenas Valley and T-II and T-I in the Talari Valley) represents a set of 10 samples collected from each site in 2000 and 2001. The ^{36}Cl exposure ages (ka) are also marked for each sample and sample site. The ages in red font are treated as outliers. The white box represents the extent of Figure 5A. (For interpretation of the references to color in this figure legend, the reader is referred to the web version of this article.)

cosmogenic ^{36}Cl surface exposure dating. Six samples were collected from moraines within the cirque of the Morrenas Valley (M-1) in 1998 (CS-0 to 5) to test the feasibility of using ^{36}Cl surface exposure dating in this area (Figs. 2 and 3A). Then, 50 samples were collected from three moraines (M-4, M-3, and M-2) below the cirque in the Morrenas Valley and from two moraines in the Talari Valley (T-II and T-I) in 2000 and 2001 (10 samples from each moraine; Figs. 2 and 3). Chemical compositions of the samples we collected plot as diorite on a TAS (Total Alkali Silica) diagram for plutonic rocks (Rippington et al., 2008). Approximately 1000 g of rock fragments was chipped from the surface of each selected boulder using hammers and chisels. We measured the latitude, longitude, and altitude information individually using a GPS unit for the six samples (CS-0 to 5) within the cirque of the Morrenas Valley. For other samples, we measured GPS locations of the bottom and the top of each set along the moraine ridge and used the average GPS location for all samples in each set. We did not keep individual notes, such as the size and height above the ground, on individual boulders. All boulders we collected were not ideally large and landmark boulders, but they were the best we could find on top of each moraine.

Samples were processed at Purdue Rare Isotope Measurement Laboratory (PRIME Lab), Purdue University, and in the cosmogenic sample preparation lab in the Laboratory of Paleoenvironmental Research at the University of Tennessee. We used the whole rock for the ^{36}Cl analysis. Each sample was first crushed and then leached to remove organic matter. After that, 15 g of well-mixed material from each sample was sent to Minerals Analytical at SGS Canada for elemental analysis, and approximately 30 g was dissolved using low Cl HF. About 1.0 mg ^{35}Cl spike carrier was added to each sample to measure the ^{35}Cl/^{37}Cl and ^{36}Cl/^{35}Cl ratios. Then, silver nitrate ($AgNO_3$) was added to precipitate silver chloride (AgCl). Each sample was then eluted through anion exchange chromatography to purify the silver chloride. The purified silver chloride of each sample was loaded into a holder (Cu covered by AgBr) and sent to the PRIME Lab for accelerator mass spectrometry (AMS) measurement.

https://doi.org/10.1017/qua.2018.133 Published online by Cambridge University Press

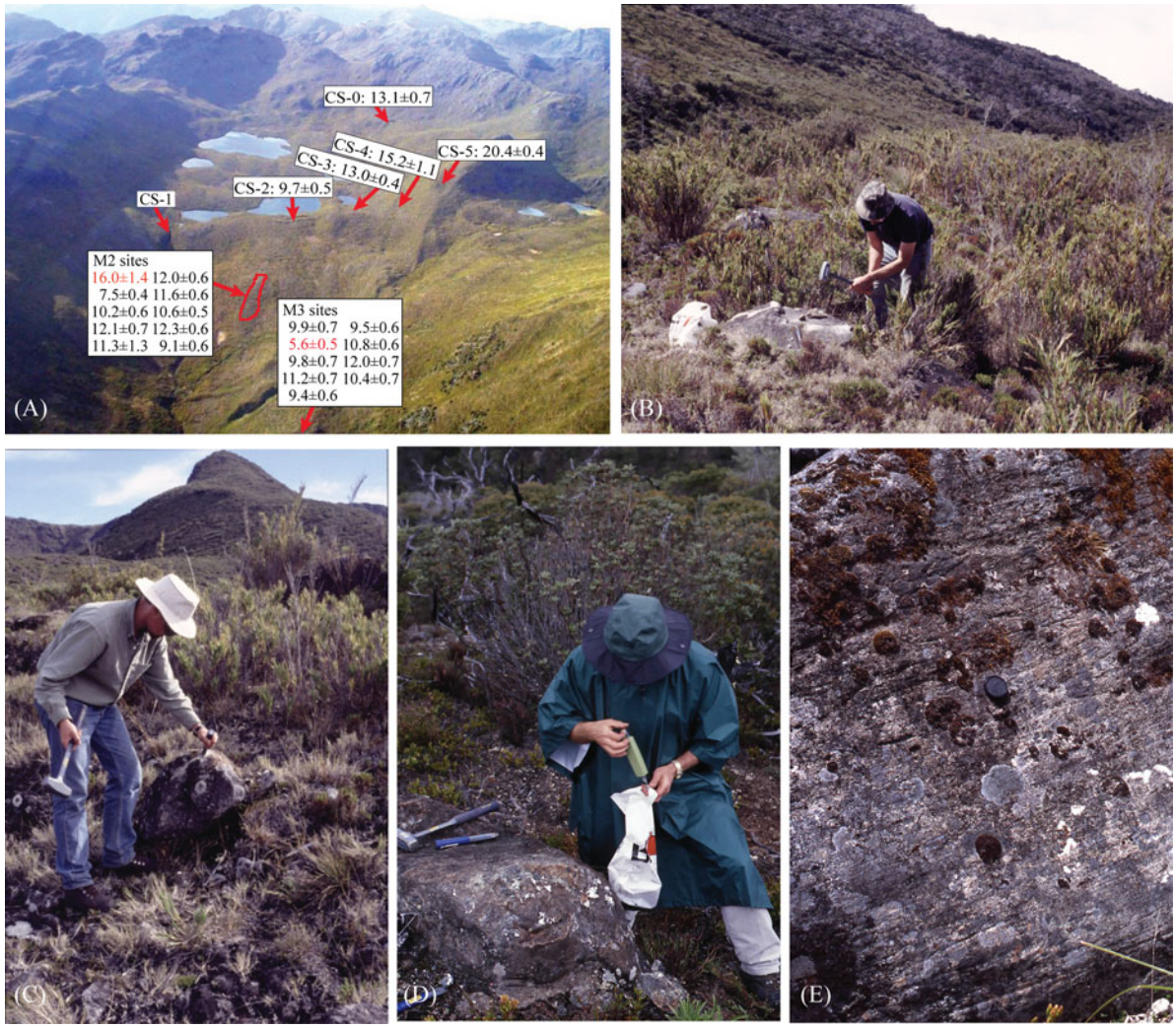

Figure 3. (color online) (A) Photo taken from a small plane, looking south up the Morrenas Valley (marked with the locations and ^{36}Cl exposure ages [ka] of the samples within the cirque [CS-0 to 5] collected in 1998 and of the M-2 and M-3 sample sites). (B–D) Field photos of sampling boulders for ^{36}Cl surface exposure dating. (E) A bedrock surface with glacial striations in the Talari Valley. Photo credits: Luis González Arce, Carol Harden, and Sally Horn.

Exposure age calculations

Cosmogenic ^{36}Cl is produced by multiple reaction pathways: spallation and muon-induced reactions of Ca, K, Fe, and Ti and thermal and epithermal neutron-capture reactions of ^{35}Cl (Marrero et al., 2016a, 2016b). The spallation is caused by the collision of high-energy neutrons with the nuclei of atoms. This reaction dominates the nuclide production at the surface and decreases exponentially with depth (Gosse and Phillips, 2001). The muon production is minor at the surface, but it can be significant for samples from depth profiles or with high erosion rates (Marrero et al., 2016a). In addition to the spallation and muon-induced productions, ^{36}Cl can also be produced by the thermal and epithermal neutron capture of ^{35}Cl (Gosse and Phillips, 2001; Marrero et al., 2016a). This production is related to the effective cross sections of ^{35}Cl and other absorbing elements and their abundances (Swanson and Caffee, 2001). The concentrations of Ca, K, Fe, Ti, and certain elements (e.g., Li, Cl, B, Cf, Sm, Gd, U, and Th) in rock samples can influence ^{36}Cl production rates (Phillips et al., 2001; Schimmelpfennig et al., 2009; Dunai, 2010). We measured the whole-rock chemical compositions for all samples (listed in Supplementary Table 1). The Cl concentration for each sample was determined by the isotope dilution mass spectrometry method, which is commonly used for ^{36}Cl analysis (Desilets et al., 2006).

We calculated ^{36}Cl exposure ages using the online ^{36}Cl Exposure Age Calculator (CRONUScalc) (Marrero et al., 2016b; Version 2.0, http://cronus.cosmogenicnuclides.rocks/2.0/html/cl/, last accessed on July 20, 2018). CRONUScalc was developed by the CRONUS-Earth project (Cosmic-Ray Produced Nuclide Systematics on Earth project) and incorporates multiple scaling models, including those recently released by Lifton et al. (2014), for the age calculation of multiple cosmogenic nuclides (e.g., ^{10}Be, ^{26}Al, ^{36}Cl, ^{3}He, and ^{14}C). For ^{36}Cl, this online calculator requires inputs that include scaling model, sample location, topographic shielding factor, erosion rate, sample thickness, rock density, and

https://doi.org/10.1017/qua.2018.133 Published online by Cambridge University Press

elemental concentrations. The ^{36}Cl exposure ages calculated by CRONUScalc are based on seven available scaling models: the Lal (1991)/Stone (2000) scaling model (denoted St in the calculator); the geomagnetically corrected version of the St model (Lm; Nishiizumi et al., 1989); three scaling models based on the global neutron monitor data (Du [Dunai, 2000, 2001], Li [Lifton et al., 2008, 2005], and De [Desilets and Zreda, 2003; Desilets et al., 2006]); and two versions of the newly introduced Lifton-Sato-Dunai (LSD) physics-based scaling model (Lifton et al., 2014)—a flux-based version (Sf) and a version incorporating nuclide-dependent and energy-dependent reaction cross sections (SA). The production rates of ^{36}Cl are based on the most recent and systematic calibration using a set of primary and secondary calibration sites in the CRONUS-Earth project (Marrero et al., 2016a). Marrero et al. (2016a, p. 201) provided detailed ^{36}Cl production rates used for different scaling models.

The topographic shielding factor for each sample was calculated in ArcGIS using a 90 m Shuttle Radar Topography Mission digital elevation model (http://srtm.csi.cgiar.org, last accessed on July 20, 2018) following the method described by Li (2013). The rock density was assigned as 2.65 g/cm^3. The calculation was based on the assumption of zero surface erosion. For each calculated exposure age, CRONUScalc reports two types of uncertainties (1-sigma): internal and external. The internal uncertainty is related to the uncertainties in sample measurements (e.g., sample weight, AMS measurement, and chemical compositions) and is used for local comparisons of the ^{36}Cl exposure ages. The external uncertainty also includes the uncertainties in the production rates and scaling model and can be used to compare exposure ages from other nuclides or dating techniques (Balco et al., 2008). In the following discussion, we use the internal uncertainty for ^{36}Cl age comparison and analysis in this area and the external uncertainty for the comparison with other ages.

Exposure ages of boulders on a moraine may be scattered because of measurement uncertainties, prior-glacial exposure (nuclide inheritance), and postglacial denudation processes (Balco et al., 2008; Heyman et al., 2011; Li et al., 2014). We plotted all exposure ages from the same moraine as a probability density function (PDF) to visually assess age clusters and scatter. We also used the Grubbs test (Grubbs, 1950) to detect the outliers of the ages. The Grubbs test is a statistical method to detect whether the maximum or minimum value of a univariate data set (following an approximately normal distribution) is an outlier based on the comparison of the z-score of each sample and the threshold z-score at the 95% confidence level. The z-score of each sample is defined as follows: (sample age − mean age) / standard deviation of all ages. If the absolute value of the z-score for a sample is larger than the absolute value of the threshold z-score, this sample is treated as an outlier.

After removing the outlier(s), we calculated the reduced chi-square statistic (χ^2_R) to test if the age scatter was because of measurement uncertainty (Balco, 2011; Li et al., 2014; Chen et al., 2015). If $\chi^2_R < 1$, the scatter is likely only because of measurement errors, and in this case, we assigned the weighted mean of these ages as the age of the moraine. If $\chi^2_R > 1$, the scatter is likely affected by moraine degradation (partial shielding) or prior exposure (nuclide inheritance) processes. In this case, we assigned the age of the moraine based on the relative geomorphic sequence and the dominant geomorphic process that the moraine had likely experienced.

Applegate et al. (2010) developed two models (the degradation model and the inheritance model) to simulate the scatter patterns of exposure ages caused by moraine degradation and prior exposure, respectively. Moraine degradation likely produces a negatively skewed distribution of apparent exposure ages, and the oldest age is likely close to the formation age of the moraine, whereas inheritance produces a positively skewed distribution, and the youngest age is likely close to the formation age of the moraine (Applegate et al., 2010). Applegate et al. (2012) demonstrated that the age of a moraine could be determined based on which of these two models showed the best fit for the measured exposure ages from a single moraine. However, these models were developed based on ^{10}Be surface exposure dating in which nuclide production is dominated by spallation and muon reactions that have exponentially decreasing patterns with depth. The nuclide production for ^{36}Cl is more complicated, especially with the production from the thermal and epithermal neutron-capture reactions of ^{35}Cl. Nuclide production from the thermal and epithermal-capture reactions is relatively lower at the surface (because of atmosphere-ground interaction) and increases with depth to roughly 15–20 cm and then decreases with depth (Gosse and Phillips, 2001; Marrero et al., 2016b). In addition, ^{36}Cl exposure ages based on whole-rock analysis are affected by the chemical composition and element concentrations of individual samples, so that the fraction of the nuclide production from the thermal and epithermal-capture reactions varies for different samples. Thus, the distribution pattern of ^{36}Cl exposure ages may not follow the patterns simulated using the two geomorphic models developed by Applegate et al. (2010).

Based on a global data set of surface exposure dates, Heyman et al. (2011) suggested that degradation is more common than inheritance on moraines produced by alpine glaciers. Given the relatively high precipitation in our study area, the moraines we sampled were likely affected by postglacial degradation and exhumation processes. Therefore, we tentatively use the oldest age (after removing the outlier) to interpret the age of the moraine when the age scatter is relatively large ($\chi^2_R > 1$). This choice is consistent with the tendency of moraine degradation to produce apparently younger exposure ages (Heyman et al., 2011).

RESULTS AND AGE INTEPRETATION

We obtained 49 ^{36}Cl exposure ages to constrain the timing of glacial events on Cerro Chirripó, Costa Rica (Table 1; seven samples were lost or did not produce reliable measurements). The exposure ages derived for different scaling models can be

https://doi.org/10.1017/qua.2018.133 Published online by Cambridge University Press

Table 1. Measured ^{36}Cl concentrations and calculated exposure ages from the Morrenas and Talari Valleys.

Location	Sample ID	Latitude	Longitude	Elevation (m asl)	Topographic shielding	Cl (ppm)	^{36}Cl concentration (10^3 atoms/g)	Exposure age De (ka)	Exposure age Du (ka)	Exposure age Li (ka)	Exposure age Lm (ka)	Exposure age SA (ka)	Exposure age Sf (ka)	Exposure age St (ka)
Talari Valley	T-I–2	9°27.12’	−83°30.30’	3357	0.9880	1.4	238 ± 10	13.6 ± 2.4(0.6)	14.0 ± 2.4(0.6)	14.2 ± 1.4(0.5)	15.0 ± 1.1(0.6)	15.2 ± 0.9(0.6)	15.2 ± 1.0(0.6)	15.3 ± 1.3(0.6)
	T-I–3	9°27.12’	−83°30.30’	3357	0.9880	5.1	550 ± 73	40.9 ± 6.1(4.2)	43.3 ± 7.5(5.3)	41.0 ± 5.0(4.2)	42.8 ± 5.5(5.0)	42.7 ± 5.1(4.8)	42.8 ± 5.2(4.9)	53.9 ± 8.5(7.7)
	T-I–4	9°27.12’	−83°30.30’	3357	0.9880	1.1	317 ± 14	14.2 ± 2.8(0.6)	14.7 ± 2.9(0.6)	14.8 ± 1.6(0.6)	16.3 ± 1.4(0.7)	16.4 ± 1.2(0.7)	16.3 ± 1.3(0.7)	16.7 ± 1.6(0.7)
	T-I–6	9°27.12’	−83°30.30’	3357	0.9880	0.3	250 ± 26	10.4 ± 2.6(1.2)	10.7 ± 2.5(1.2)	10.9 ± 1.9(1.2)	12.0 ± 1.5(1.2)	12.1 ± 1.4(1.2)	12.1 ± 1.5(1.2)	12.2 ± 1.6(1.3)
	T-I–7	9°27.12’	−83°30.30’	3357	0.9880	16.1	289 ± 13	11.7 ± 2.2(0.5)	12.0 ± 2.2(0.5)	12.2 ± 1.3(0.5)	13.5 ± 1.2(0.6)	14.0 ± 1.0(0.6)	13.5 ± 1.1(0.6)	13.6 ± 1.3(0.6)
	T-I–8	9°27.12’	−83°30.30’	3357	0.9880	18.1	300 ± 12	11.0 ± 2.0(0.5)	11.0 ± 2.0(0.5)	11.2 ± 1.3(0.5	12.1 ± 1.0(0.5)	12.3 ± 0.9(0.5)	12.2 ± 0.9(0.5)	12.3 ± 1.1(0.5)
	T-I–9	9°27.12’	−83°30.30’	3357	0.9880	28.2	355 ± 15	10.3 ± 1.8(0.5)	10.6 ± 1.8(0.5)	10.8 ± 1.2(0.5)	11.0 ± 1.0(0.5)	11.7 ± 0.9(0.5)	11.7 ± 0.9(0.5)	12.0 ± 1.0(0.5)
	T-I–10	9°27.12’	−83°30.30’	3357	0.9880	1.3	406 ± 15	14.0 ± 3.0(0.5)	14.0 ± 3.0(0.5)	14.2 ± 1.7(0.5)	15.8 ± 1.4(0.6)	15.9 ± 1.1(0.6)	15.7 ± 1.2(0.6)	16.1 ± 1.6(0.6)
	T-II–1	9°27.18’	−83°30.30’	3349	0.9811	17.8	718 ± 129	22.0 ± 5.0(3.7)	23.4 ± 5.5(4.1)	22.9 ± 4.3(3.8)	24.8 ± 4.1(3.8)	24.8 ± 3.9(3.7)	24.7 ± 3.9(3.7)	27.5 ± 5.5(5.1)
	T-II–2	9°27.18’	−83°30.30’	3349	0.9811	8.2	225 ± 34	7.0 ± 2.0(1.2)	8.0 ± 2.0(1.2)	7.8 ± 1.6(1.3)	8.8 ± 1.7(1.5)	8.8 ± 1.7(1.6)	8.7 ± 1.7(1.6)	9.1 ± 1.6(1.4)
	T-II–5	9°27.18’	−83°30.30’	3349	0.9811	2.9	521 ± 217	18.8 ± 7.3(6.6)	19.4 ± 7.3(6.7)	19.3 ± 6.4(6.2)	20.6 ± 6.7(6.6)	20.7 ± 6.6(6.5)	20.6 ± 6.5(6.4)	22.1 ± 9.6(9.4)
	T-II–6	9°27.18’	−83°30.30’	3349	0.9811	2.8	404 ± 27	14.9 ± 2.6(0.9)	15.3 ± 2.8(1.0)	15.4 ± 1.7(1.0)	16.5 ± 1.5(1.1)	16.8 ± 1.3(1.1)	16.7 ± 1.4(1.1)	17.0 ± 1.7(1.2)
	T-II–8	9°27.18’	−83°30.30’	3349	0.9811	8.9	348 ± 13	14.0 ± 2.3(0.5)	14.4 ± 2.3(0.5)	14.6 ± 1.4(0.5)	15.5 ± 1.1(0.6)	15.7 ± 1.0(0.6)	16.0 ± 1.0(0.6)	15.9 ± 1.3(0.6)
	T-II–9	9°27.18’	−83°30.30’	3349	0.9811	4.1	372 ± 14	12.7 ± 2.5(0.5)	13.0 ± 2.5(0.5)	13.3 ± 1.5(0.5)	14.3 ± 1.1(0.5)	14.6 ± 0.9(0.5)	14.5 ± 1.0(0.5)	14.6 ± 1.2(0.6)
	T-II–10	9°27.18’	−83°30.30’	3349	0.9811	2.0	346 ± 19	12.2 ± 2.3(0.7)	12.6 ± 2.4(0.7)	12.7 ± 1.5(0.7)	13.7 ± 1.2(0.7)	14.0 ± 1.0(0.7)	13.8 ± 1.1(0.8)	13.9 ± 1.3(0.8)
Morrenas Valley	M-2–1	9°30.00’	−83°29.34’	3462	0.9869	174.6	1010 ± 88	14.2 ± 2.7(1.2)	14.6 ± 2.8(1.2)	14.8 ± 2.4(1.2)	15.7 ± 2.9(1.3)	16.0 ± 2.8(1.4)	15.9 ± 2.8(1.4)	16.1 ± 3.2(1.5)
	M-2–2	9°30.00’	−83°29.34’	3462	0.9869	260.2	593 ± 31	6.6 ± 1.1(0.3)	6.8 ± 1.2(0.3)	6.8 ± 1.0(0.3)	7.5 ± 1.5(0.4)	7.5 ± 1.4(0.4)	7.4 ± 1.3(0.4)	7.9 ± 1.5(0.4)
	M-2–3	9°30.00’	−83°29.34’	3462	0.9869	218.0	657 ± 35	8.7 ± 1.9(0.5)	9.0 ± 1.8(0.5)	9.1 ± 1.9(0.6)	10.1 ± 2.2(0.6)	10.2 ± 1.9(0.6)	10.0 ± 2.0(0.6)	10.0 ± 2.0(0.6)
	M-2–4	9°30.00’	−83°29.34’	3462	0.9869	134.4	465 ± 25	10.7 ± 1.9(0.6)	11.0 ± 1.8(0.6)	11.3 ± 1.6(0.7)	12.1 ± 1.7(0.6)	12.1 ± 1.5(0.7)	12.3 ± 1.6(0.7)	12.3 ± 1.8(0.7)
	M-2–5	9°30.00’	−83°29.34’	3462	0.9869	75.4	381 ± 39	10.0 ± 2.0(0.5)	10.4 ± 1.9(1.2)	10.6 ± 1.8(1.3)	11.1 ± 1.9(1.3)	11.3 ± 1.7(1.3)	11.3 ± 1.8(1.3)	11.3 ± 1.8(1.2)
	M-2–6	9°30.00’	−83°29.34’	3462	0.9869	295.6	1048 ± 46	10.6 ± 2.2(0.5)	10.9 ± 2.2(1.2)	11.1 ± 2.1(0.6)	12.1 ± 2.2(0.5)	12.0 ± 2.0(0.6)	12.2 ± 2.1(0.5)	12.3 ± 2.4(0.6)
	M-2–7	9°30.00’	−83°29.34’	3462	0.9869	239.9	834 ± 38	10.0 ± 2.0(0.5)	10.0 ± 2.0(0.5)	10.5 ± 1.9(0.6)	11.5 ± 2.1(0.6)	11.6 ± 1.9(0.6)	11.5 ± 1.9(0.6)	11.6 ± 2.1(0.5)
	M-2–8	9°30.00’	−83°29.34’	3462	0.9869	347.4	1024 ± 43	9.0 ± 2.0(0.5)	9.0 ± 2.0(0.5)	10.0 ± 2.0(0.5)	10.5 ± 2.2(0.5)	10.6 ± 2.1(0.5)	10.5 ± 2.1(0.5)	10.7 ± 2.1(0.5)
	M-2–9	9°30.00’	−83°29.34’	3462	0.9869	76.2	401 ± 20	11.3 ± 1.9(0.6)	11.0 ± 2.0(0.6)	11.7 ± 1.6(0.6)	12.0 ± 1.6(0.6)	12.3 ± 1.6(0.6)	12.3 ± 1.5(0.6)	12.3 ± 1.7(0.6)
	M-2–10	9°30.00’	−83°29.34’	3462	0.9869	405.7	1021 ± 57	7.8 ± 1.7(0.5)	8.1 ± 1.7(0.5)	8.1 ± 1.7(0.5)	9.0 ± 2.2(0.6)	9.1 ± 2.1(0.6)	9.0 ± 2.0(0.6)	9.0 ± 2.0(0.6)
	M-3–1	9°30.30’	−83°29.52’	3391	0.9751	393.3	1031 ± 60	8.4 ± 1.9(0.6)	8.8 ± 1.9(0.6)	9.0 ± 2.0(0.6)	9.8 ± 2.4(0.7)	9.9 ± 2.2(0.7)	9.8 ± 2.2(0.7)	10.0 ± 2.1(0.6)
	M-3–2	9°30.30’	−83°29.52’	3391	0.9751	506.1	709 ± 80	5.0 ± 1.0(0.5)	4.9 ± 1.1(0.6)	5.2 ± 0.9(0.5)	6.0 ± 1.0(0.5)	5.6 ± 0.9(0.5)	5.5 ± 0.9(0.5)	5.4 ± 1.3(0.7)
	M-3–3	9°30.30’	−83°29.52’	3391	0.9751	256.2	758 ± 43	8.4 ± 1.8(0.5)	8.7 ± 1.8(0.6)	8.8 ± 1.8(0.6)	9.7 ± 2.1(0.7)	9.8 ± 1.9(0.7)	9.7 ± 1.9(0.7)	10.0 ± 1.9(0.6)
	M-3–5	9°30.30’	−83°29.52’	3391	0.9751	349.8	1045 ± 54	9.6 ± 2.2(0.6)	9.9 ± 2.1(0.6)	10.1 ± 2.1(0.6)	11.0 ± 2.4(0.7)	11.2 ± 2.2(0.7)	11.1 ± 2.2(0.6)	11.2 ± 2.3(0.6)
	M-3–6	9°30.30’	−83°29.52’	3391	0.9751	456.7	1106 ± 60	8.0 ± 1.8(0.5)	8.3 ± 1.9(0.5)	8.4 ± 1.8(0.5)	9.2 ± 2.3(0.6)	9.4 ± 2.1(0.6)	9.3 ± 2.2(0.6)	9.6 ± 2.1(0.6)
	M-3–7	9°30.30’	−83°29.52’	3391	0.9751	399.1	999 ± 52	8.1 ± 1.8(0.5)	8.4 ± 1.8(0.5)	8.5 ± 1.8(0.5)	9.4 ± 2.3(0.6)	9.5 ± 2.1(0.6)	9.4 ± 2.1(0.6)	10.0 ± 2.0(0.5)
	M-3–8	9°30.30’	−83°29.52’	3391	0.9751	327.3	964 ± 49	9.3 ± 2.1(0.6)	9.6 ± 2.1(0.6)	9.8 ± 2.1(0.6)	10.7 ± 2.3(0.6)	10.8 ± 2.2(0.6)	10.7 ± 2.2(0.7)	10.9 ± 2.2(0.6)
	M-3–9	9°30.30’	−83°29.52’	3391	0.9751	276.7	892 ± 47	9.9 ± 2.1(0.6)	10.2 ± 2.1(0.6)	10.0 ± 2.0(0.6)	11.4 ± 2.3(0.7)	12.0 ± 2.0(0.7)	11.5 ± 2.1(0.7)	11.5 ± 2.2(0.6)
	M-3–10	9°30.30’	−83°29.52’	3391	0.9751	425.5	1145 ± 63	8.9 ± 2.1(0.6)	9.2 ± 2.1(0.6)	9.3 ± 2.1(0.7)	10.3 ± 2.4(0.7)	10.4 ± 2.2(0.7)	10.3 ± 2.3(0.7)	10.5 ± 2.2(0.6)
	M-4–1	9°30.78’	−83°29.76’	3310	0.9753	321.7	4575 ± 154	44.5 ± 7.9(1.4)	48.0 ± 11.0(1.9)	45.3 ± 7.9(1.6)	51.0 ± 12.0(2.1)	50.0 ± 11.0(2.2)	50.0 ± 11.0(2.2)	63.0 ± 13.0(2.3)
	M-4–2	9°30.78’	−83°29.76’	3310	0.9753	339.0	413 ± 13	4.8 ± 0.8(0.1)	4.7 ± 0.8(0.2)	5.0 ± 0.7(0.1)	5.3 ± 0.9(0.2)	5.3 ± 0.7(0.1)	5.3 ± 0.7(0.1)	5.1 ± 1.0(0.2)
	M-4–3	9°30.78’	−83°29.76’	3310	0.9753	367.3	1216 ± 36	12.6 ± 2.5(0.4)	12.9 ± 2.6(0.4)	13.2 ± 2.4(0.4)	14.2 ± 2.7(0.4)	14.4 ± 2.3(0.4)	14.3 ± 2.4(0.4)	14.4 ± 2.9(0.4)
	M-4–4	9°30.78’	−83°29.76’	3310	0.9753	397.6	2415 ± 106	21.1 ± 3.3(0.8)	22.0 ± 4.1(0.9)	21.7 ± 3.3(0.8)	23.4 ± 4.4(1.0)	23.6 ± 3.8(0.9)	23.4 ± 3.8(0.9)	25.7 ± 5.3(1.2)
	M-4–5	9°30.78’	−83°29.76’	3310	0.9753	284.9	1857 ± 73	20.6 ± 2.9(0.6)	21.4 ± 3.4(0.8)	21.2 ± 2.8(0.7)	22.5 ± 3.8(0.8)	22.7 ± 3.4(0.8)	22.6 ± 3.4(0.8)	24.7 ± 4.6(1.0)
	M-4–6	9°30.78’	−83°29.76’	3310	0.9753	268.5	1133 ± 61	14.6 ± 2.4(0.7)	15.0 ± 2.5(0.8)	15.2 ± 2.2(0.8)	16.0 ± 2.7(0.9)	16.4 ± 2.5(0.9)	16.3 ± 2.5(0.9)	16.5 ± 2.9(0.9)

Table 1. Continued.

Location	Sample ID	Latitude	Longitude	Elevation (m asl)	Topographic shielding	^{36}Cl							
						Cl (ppm)	concentration (10^3 atoms/g)	Exposure age De (ka)	Exposure age Du (ka)	Exposure age Li (ka)	Exposure age Lm (ka)	Exposure age SA (ka)	Exposure age Sf (ka)	Exposure age St (ka)
	M-4–7	9°30.78’	−83°29.76’	3310	0.9753	348.9	998 ± 58	9.7 ± 2.2(0.7)	10.0 ± 2.1(0.7)	10.2 ± 2.1(0.7)	11.1 ± 2.4(0.7)	11.3 ± 2.2(0.7)	11.2 ± 2.2(0.7)	11.3 ± 2.3(0.7)
	M-4–8	9°30.78’	−83°29.76’	3310	0.9753	194.8	944 ± 38	14.1 ± 2.3(0.6)	14.5 ± 2.4(0.6)	15.0 ± 2.0(0.5)	15.5 ± 2.4(0.6)	15.9 ± 2.2(0.6)	15.8 ± 2.3(0.6)	16.0 ± 2.7(0.7)
	M-4–9	9°30.78’	−83°29.76’	3310	0.9753	123.1	767 ± 39	14.9 ± 2.1(0.7)	15.3 ± 2.4(0.8)	15.4 ± 1.9(0.8)	16.3 ± 2.3(0.8)	17.0 ± 2.0(0.8)	16.6 ± 2.1(0.8)	16.8 ± 2.4(0.9)
	M-4–10	9°30.78’	−83°29.76’	3310	0.9753	196.4	1192 ± 62	17.5 ± 2.8(0.9)	18.0 ± 3.0(0.9)	18.2 ± 2.5(0.8)	19.3 ± 2.6(0.8)	19.5 ± 2.3(0.8)	19.4 ± 2.3(0.8)	20.2 ± 3.5(1.1)
Morrenas cirque (M-1)	CS–0	9°29.28’	−83°29.28’	3551	0.9745	64.0	489 ± 24	11.5 ± 1.7(0.6)	11.8 ± 1.7(0.6)	12.0 ± 1.3(0.6)	12.8 ± 1.4(0.7)	13.1 ± 1.4(0.7)	13.0 ± 1.4(0.7)	13.1 ± 1.5(0.7)
	CS–2	9°29.82’	−83°29.28’	3482	0.9886	382.3	1015 ± 40	8.3 ± 1.8(0.4)	8.6 ± 1.8(0.4)	8.7 ± 1.8(0.4)	9.6 ± 2.2(0.5)	9.7 ± 2.1(0.5)	9.6 ± 2.1(0.5)	10.0 ± 2.0(0.4)
	CS–3	9°29.76’	−83°29.40’	3513	0.9865	78.4	537 ± 17	11.4 ± 1.7(0.4)	11.7 ± 1.7(0.4)	11.9 ± 1.3(0.4)	12.7 ± 1.4(0.4)	13.0 ± 1.3(0.4)	12.9 ± 1.4(0.4)	12.9 ± 1.4(0.4)
	CS–4	9°29.70’	−83°29.40’	3558	0.9774	89.1	628 ± 51	13.5 ± 2.2(1.1)	13.8 ± 2.2(1.1)	14.0 ± 1.8(1.1)	15.0 ± 1.9(1.1)	15.2 ± 1.7(1.1)	15.1 ± 1.7(1.1)	15.4 ± 2.2(1.3)
	CS–5	9°29.70’	−83°29.46’	3590	0.9947	123.1	1115 ± 29	18.5 ± 2.5(0.4)	19.1 ± 2.5(0.4)	19.1 ± 1.9(0.4)	20.0 ± 2.0(0.4)	20.4 ± 1.7(0.4)	20.3 ± 1.8(0.4)	22.0 ± 3.0(0.6)

The exposure ages were calculated using the CRONUS online ^{36}Cl exposure age calculator (Marrero et al., 2016b; Version 2.0; http://cronus.cosmogenicnuclides.rocks/2.0/html/cl/, last accessed on July 20, 2018) based on the assumption of zero surface erosion. The exposure ages were calculated for seven scaling models: Du (Dunai, 2000, 2001), Li (Lifton et al., 2005, 2008), De (Desilets and Zreda, 2003; Desilets et al., 2006), Lm (Nishiizumi et al., 1989; Lal, 1991; Stone, 2000), SA (Lifton et al., 2014), Sf (Lifton et al., 2014), and St (Lal, 1991; Stone, 2000), respectively. The production rates of ^{36}Cl are based on the most recent and systematic calibration using primary and secondary calibration sites in the CRONUS-Earth project (Marrero et al., 2016a). The topographic shielding factor for each sample was calculated using a 90 m Shuttle Radar Topography Mission digital elevation model based on Li (2013). The sample thickness of 4 cm and the rock density of 2.65 g/cm^3 are used in the calculation. The external uncertainty and internal uncertainty (in the parentheses) are reported for each exposure age (1-sigma error).

divided into two groups: the exposure ages calculated based on neutron monitor–based scaling models (Du, De, and Li) and the ages based on the other four scaling models (St, Lm, Sf, and SA). The age differences within each group are minor (<5% for most samples), whereas the differences between these two groups are >10% for most samples. The CRONUS-Earth project suggests that the LSD-based (SA and Sf) and the Lal-based scaling models (St and Lm) have better fits for the calibration data than the neutron monitor–based scaling models (Du, De, and Li) (Borchers et al., 2015; Marrero et al., 2016a). Therefore, we mainly use the exposure ages calculated using the nuclide-dependent LSD scaling model (SA) in the following discussion. Recent studies indicate that this scaling model produces the best fit for the calibration data (Borchers et al., 2015; Marrero et al., 2016a, 2016b) and has the possibility for future incorporation of updates to the excitation functions and findings of other physics-based research (Marrero et al., 2016b). Note that the differences between the ages derived from the SA model and the widely used Lm model in the literature are <2.5% for most samples (45 out of the total 49 samples). Thus, the difference caused by these two scaling models would not likely have important effects on the interpretation of the results.

Thirty-four ^{36}Cl exposure ages were obtained from four moraine complexes in the Morrenas Valley. Ten exposure ages from the Chirripó IV moraine (M-4) range from 50.0 ± 2.2 to 5.3 ± 0.1 ka (internal uncertainty). The PDF shows a multimode distribution of ages, and the oldest age of 50.0 ± 2.2 ka and the youngest age of 5.3 ± 0.1 ka are different from the distribution of the other ages from 10 to 25 ka (Fig. 4A). The Grubbs test indicates that the oldest age of 50.0 ± 2.2 ka is an outlier, but not the youngest age of 5.3 ± 0.7 ka (Fig. 4B). The oldest age of 50.0 ± 11.0 ka likely resulted from nuclide inheritance because of prior exposure. The χ^2_R value of all these ages is 2341.7 and reduces to 1521.8 after removing the oldest age of 50.0 ± 2.2 ka. As discussed in the “Methods” section, after removing the outlier, we tentatively assigned the oldest age of 23.6 ± 0.9 ka (internal uncertainty) from the remaining ages as the formation age of this moraine because of the high scatter of these ages (χ^2_R>>1).

Nine exposure ages from the Chirripó III moraine (M-3) range from 12.0 ± 0.7 to 5.6 ± 0.5 ka. The PDF of these ages shows that ages cluster around 10.0 ka (Fig. 4C). The youngest age of 5.6 ± 0.5 ka is detected by the Grubbs test as an outlier (Fig. 4D). The χ^2_R value of the remaining ages is 1.65, indicating that these ages were still likely affected by postglacial geomorphic processes. We assigned the oldest age of 12.0 ± 0.7 ka as the age of this moraine.

Ten exposure ages from the Chirripó II moraine (M-2) range from 16.0 ± 1.4 to 7.5 ± 0.4 ka. The PDF of these ages shows that ages cluster around 12.0 ka (Fig. 4E). The Grubbs test indicates that the oldest age of 16.0 ± 1.4 ka is likely an outlier (Fig. 4F). After removing this outlier, the χ^2_R value of the remaining ages is 11.4, indicating that these ages were likely affected by postglacial geomorphic processes.

https://doi.org/10.1017/qua.2018.133 Published online by Cambridge University Press

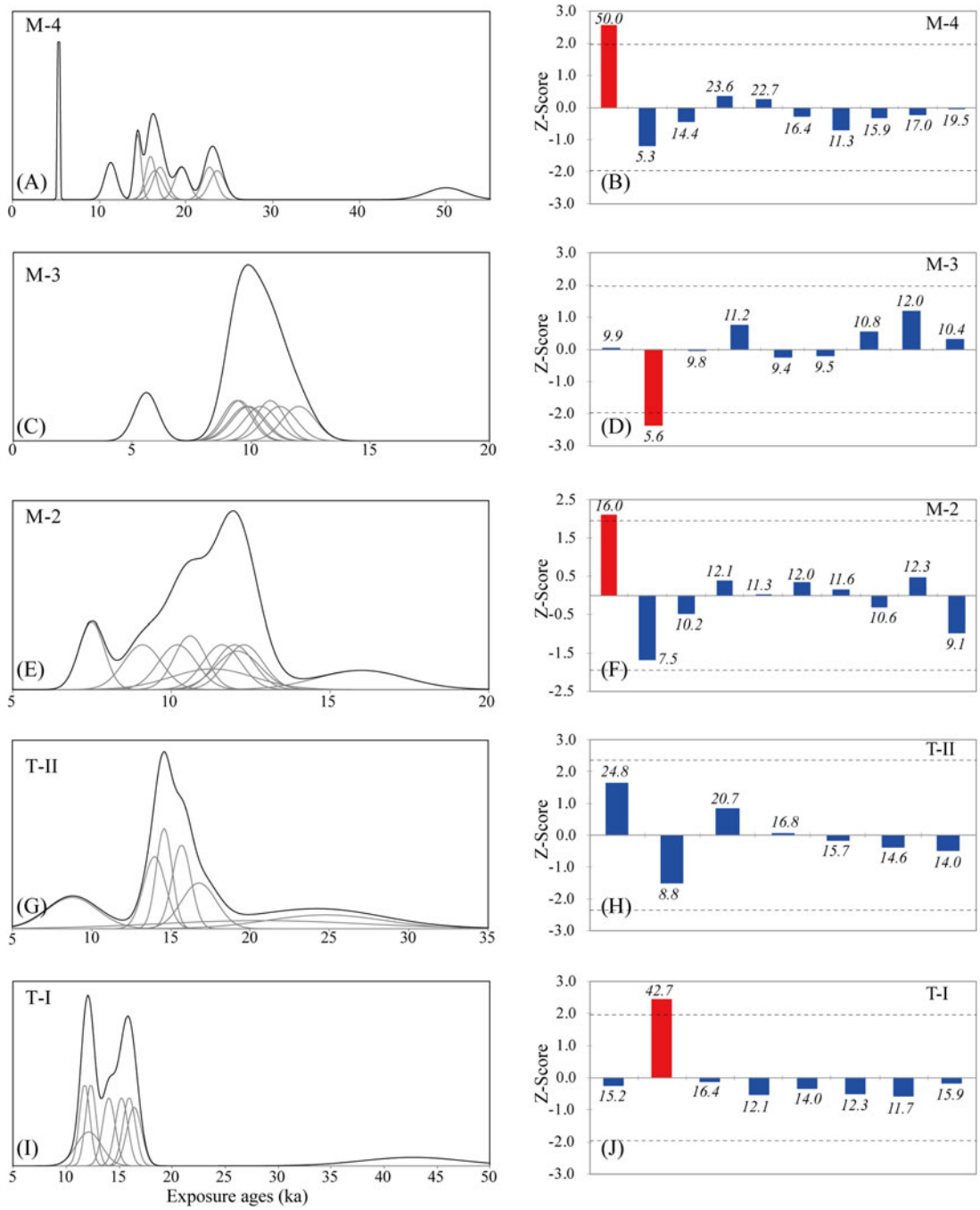

Figure 4. (color online) Probability density plots and outlier detection results based on the Grubbs test of ^{36}Cl exposure ages from five moraines in the Morrenas and Talari Valleys. Moraines in the Morrenas Valley include the M-4 moraine (A and B), the M-3 moraine (C and D), and the M-2 moraine (E and F). Moraines in the Talari Valley include the T-II moraine (G and H) and the T-I moraine (I and J). Panels A, C, E, G, and I are the probability density plots, and panels B, D, F, H, and J are the Grubbs test results for outlier detection of these moraines.

We assigned the oldest remaining age of 12.3 ± 0.6 ka as the age of this moraine.

Four exposure ages from the Chirripó I moraine complex (M-1; CS-0, 2, 3, and 4) range from 15.2 ± 1.1 to 9.7 ± 0.5 ka. We did not plot these ages as a PDF because these four samples were collected from separate moraine ridges. We also obtained an exposure age of 20.4 ± 0.4 ka (CS-5) from a higher lateral moraine on the eastern wall of the cirque. It likely corresponds to the older and most extensive Chirripó IV moraine (M-4) down the valley.

Fifteen ^{36}Cl exposure ages were obtained from the two moraines in the Talari Valley. Seven exposure ages from the lower Talari moraine (T-II) range from 24.8 ± 3.7 to 8.8 ± 1.6 ka. The PDF of these ages (Fig. 4G) shows that ages cluster around 14.8 ka; the Grubbs test detects no outliers (Fig. 4H). The χ^2_R value of these ages is 9.5, indicating that

https://doi.org/10.1017/qua.2018.133 Published online by Cambridge University Press

these ages were likely affected by postglacial moraine degradation. We assigned the oldest age of 24.8 ± 3.7 ka as the age of this moraine.

Eight ages from the upper Talari moraine (T-I) range from 42.7 ± 5.1 to 11.7 ± 0.9 ka. The PDF of these ages (Fig. 4I) shows that ages cluster around 15.8 and 12.0 ka. The Grubbs test indicates that the oldest age of 42.7 ± 5.1 ka is likely an outlier (Fig. 4J), probably because of prior exposure of the boulder (nuclide inheritance). Removing this age from the data set reduces the χ^2_R value to 10.1, indicating that the remaining ages were still affected by postglacial degradation processes. We assigned the oldest age of 16.4 ± 0.7 ka as the age of this moraine.

DISCUSSION

Cosmogenic ^{36}Cl exposure ages

To validate the use of ^{36}Cl surface exposure dating to date glacial landforms in this area, we compared the four ^{36}Cl exposure ages (CS-0, 2, 3, and 4, using external uncertainty) for boulders on moraine ridges in the Chirripó I moraine complex with calibrated radiocarbon ages based on dates on bulk sediment and charcoal in basal sediments of three glacial lakes within the cirque of the Morrenas Valley (Horn, 1990; Orvis and Horn, 2000; Lane et al., 2011; Fig. 5A). The radiocarbon dates were recalibrated using Calib 7.0.2 (Stuiver and Reimer, 1993) and the data set of Reimer et al. (2013). Three radiocarbon dates were on material from just above the transition from mineral glacial facies to organic sediment in Lake 4 (AMS ^{14}C on organic sediment; Orvis and Horn, 2000), Lake 1 (standard ^{14}C analysis on sediment; Horn, 1990), and Lake 0A (AMS ^{14}C on charcoal; Orvis and Horn, 2000). These samples yielded calibrated age ranges (95% confidence, rounded) of 9.7–9.5 ka cal BP for Lake 4, 10.2–9.7 ka cal BP for Lake 1, and 9.9–9.5 ka cal BP for Lake 0A. Horn (1990) also obtained a standard radiocarbon date on transitional sediment (mineral silt with sparse organics) below the basal organics in Lake 1, and Lane et al. (2011) obtained an AMS date on a 2 cm section of sediment that spanned the transition from mineral to organic sediment. The calibrated age ranges for these samples are 12.4–11.3 ka cal yr BP and 11.3–11.2 ka cal yr BP, respectively.

The comparison indicates that the ^{36}Cl exposure ages are similar but as a set slightly older than the calibrated radiocarbon ages (Fig. 5B). These glacial lakes were formed after the retreat of glaciers, so the radiocarbon ages from basal lake sediments are expected to be somewhat younger than the moraine ages. On the other hand, the ^{36}Cl exposure ages are affected by the uncertainties in the production rates. As indicated by Marrero et al. (2016a), most calibration sites for production rates are from the middle and high latitudes, and the only site from tropical America, Huancané, Peru (13°S), produced high scatter results and was not included in the production rate calibration. Therefore, the production rates in low latitudes still have relatively large uncertainties. Differences of 5–10% in production rates, for example, could change the exposure age by 5–10%. However, even if the true ^{36}Cl production rates are 5–10% higher or lower than the production rates we used in the calculation, the derived ^{36}Cl exposure ages are still in agreement with the minimum-limiting ages on lake sediments. This comparison indicates that our ^{36}Cl exposure ages are reliable and can be used to constrain the glacial chronology in this area.

Our calculated exposure ages are based on the assumption of zero erosion of the boulder surface. To examine the effect of boulder surface erosion, we compared our calculated ages with ages derived using a surface erosion rate of 3 mm/ka, a potential maximum surface erosion rate used in many other studies (e.g., Abramowski et al., 2006; Koppes et al., 2008; Li et al., 2011). Surface erosion does not always result in apparently older ^{36}Cl exposure ages, because of the production of thermal and epithermal neutron reactions. For our samples, the differences in calculated ages derived using these two erosion rates were mainly <5.0% (average 2.0%) (Fig. 6). From this comparison, we conclude that boulder surface erosion does not have a significant impact on the exposure ages in our study. This interpretation is consistent with the sensitivity analysis by Marrero et al. (2016a) of the impact of different factors on ^{36}Cl exposure age. Based on analyses of calibration data sets, the researchers concluded that erosion rate is a minor contributor (1.0–2.5%) to the uncertainty of ^{36}Cl exposure age (Marrero et al., 2016a). Note that we did not assess the impact of snow cover, as there is no snow in this area in the present climate. We also did not evaluate the influence of moraine degradation, past air pressure conditions, and the water content in the environment on exposure ages (Marrero et al., 2016a), because of the lack of information. Given the apparently minor impact of surface erosion on exposure ages, the wide scatter in the ages does indicate that these moraines were likely affected by postglacial degradation and exhumation. Thus, the use of the oldest age to represent the age of each moraine is reasonable.

Glacial chronology in the Chirripó highland

The ^{36}Cl exposure ages show similar timing and extent of glacial events between the Morrenas and Talari Valleys. The exposure ages of the M-4 moraine in the Morrenas Valley are similar to the exposure ages of the T-II moraine in the Talari Valley. The oldest exposure age for the M-4 moraine, which reaches to 3310 m asl, is 23.6 ± 0.9 ka in the Morrenas Valley after excluding one outlier. In the Talari Valley, the oldest exposure age from the T-II moraine (reaches to 3349 m asl) is 24.8 ± 3.7 ka. Similar exposure ages indicate that these moraines of similar extent in two valleys were formed during the same glacial stage, confirming the interpretation of Lachniet and Seltzer (2002). Based on our cosmogenic isotope results, we place their formation at 25–23 ka, corresponding to the global last glacial maximum (LGM).

The oldest exposure ages from the M-3 and M-2 moraines in the Morrenas Valley are 12.0 ± 0.7 and 12.3 ± 0.6 ka, respectively. The four ^{36}Cl exposure ages (CS-0, 2, 3, and 4) from the M-1 moraine complex within the cirque of the

https://doi.org/10.1017/qua.2018.133 Published online by Cambridge University Press

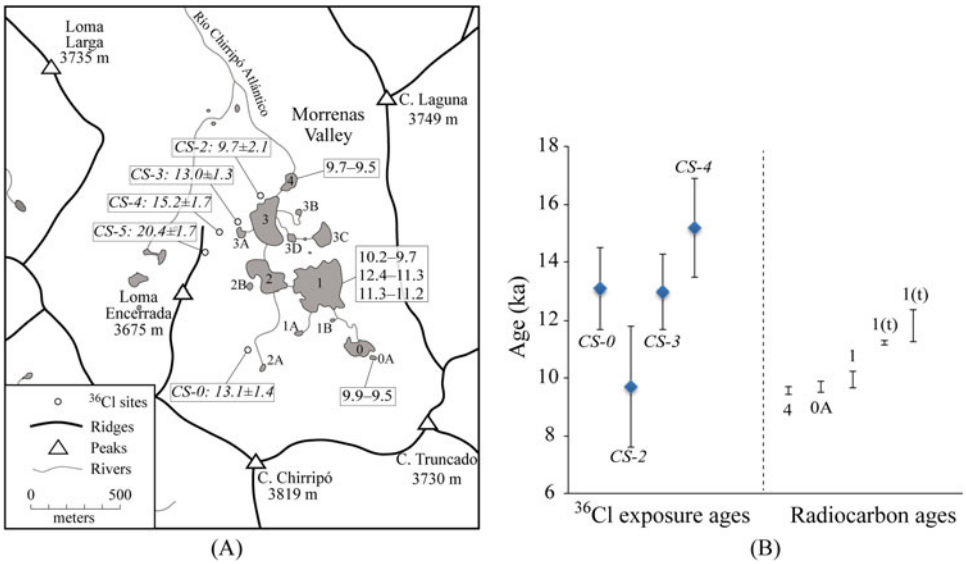

Figure 5. (color online) (A) An enlarged lake map marked with measured ^{36}Cl exposure ages (ka, with external uncertainty) and the calibrated radiocarbon age ranges (ka cal BP, 95% confidence) from basal sediments of three glacial lakes within the cirque of the Morrenas Valley. The code for each lake is based on Orvis and Horn (2000). (B) The comparison between the ^{36}Cl exposure ages and the calibrated radiocarbon age ranges. The sample ID is marked for each ^{36}Cl age. The lake code where each calibrated radiocarbon age range was dated is also marked ("t" indicates that the radiocarbon sample consisted of or included transitional sediment below the basal organics).

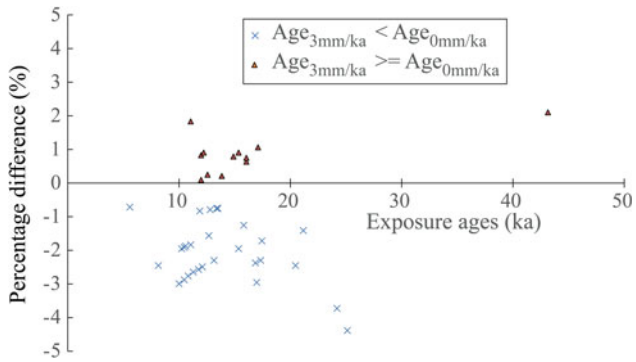

Figure 6. (color online) Scatter plot illustrating the difference (%) between the ^{36}Cl exposure ages derived under the assumption of zero surface erosion and using a surface erosion rate of 3 mm/ka.

Morrenas Valley are from 15.2 ± 1.1 to 9.7 ± 0.5 ka with two of these four ages clustering at 13 ka. The close proximity of these moraines (<2 km apart) and their similar exposure ages suggest that they were likely formed during periods of glacial retreats and standstills (15–10 ka) from the deglacial period to Early Holocene. Similarly, the oldest exposure age of the T-I moraine in the Talari Valley is 16.4 ± 0.7 ka after excluding the outlier. This moraine was also likely formed during the deglacial period. The lack of exposure ages younger than ~10 ka within the cirque of the Morrenas Valley is consistent with the interpretation of Orvis and Horn (2000), based on radiocarbon dating of lake sediments, that deglaciation of the valley was complete well before 9.7 ka cal BP.

In summary, our exposure ages suggest that all dated moraines within these two valleys were likely formed by glacial advance during the global LGM and periods of glacial retreat and standstill from the deglacial period to Early Holocene. This chronology is much younger than the polystage interpretation of Orvis and Horn (2000), who suggested that the Chirripó IV–II moraines in the Morrenas Valley could correspond to MIS 6 to MIS 2. However, our ages fit with the geomorphic interpretation of Wunsch et al. (1999), which attributed the moraines to a single cold stage. Our exposure ages are also consistent with estimates of relative age made by Lachniet and Seltzer (2002) using the evidence of the heights of weathered quartz vein pedestals on moraine boulders. Based on relatively small differences in pedestal heights, Lachniet and Seltzer (2002) concluded that their Talamanca moraines (M-4 and T-II) were probably no more than a few thousand years older than the Chirripó moraines (M-3 and T-I).

Comparison of glacial chronology with other areas

Our exposure ages indicate that the maximum glacial extent occurred in the Chirripó highland during the global LGM. Many studies have provided evidence of global LGM glacial events in the tropics and subtropics (e.g., Kaplan et al., 2007, 2008; Kull et al., 2008; Bromley et al., 2009; Hein et al., 2009, 2010; Zech et al., 2009; Glasser et al., 2011; Wesnousky et al., 2012; Carcaillet et al., 2013). These events were broadly synchronous with the global LGM advances at mid- to high latitudes in North America (Briner et al., 2005; Briner and Kaufman, 2008; Licciardi and Pierce, 2008; Phillips et al., 2009; Young et al., 2009, 2011; Rood et al., 2011; Laabs et al., 2013).

Multiproxy evidence, including isotopic records from ice cores and ^{10}Be exposure ages, indicate broadly synchronous

https://doi.org/10.1017/qua.2018.133 Published online by Cambridge University Press

retreat of LGM glaciers in both hemispheres (e.g., Schaefer et al., 2006; Denton et al., 2010; Putnam et al., 2013). Post-LGM warming was punctuated by short cooling phases during the deglacial to Holocene, which likely stalled retreat or caused glaciers to readvance. Exposure ages presented in this study indicate periods of glacial retreats and standstills from the deglacial period to Early Holocene on the Chirripó massif. Previously published chronologies indicated similar events in other tropical and subtropical areas (Vázquez-Selem and Heine, 2004; Farber et al., 2005; Zech et al., 2006; Pigati et al., 2008; Bromley et al., 2009; Hall et al., 2009; Smith et al., 2009; Zech et al., 2009; Kaplan et al., 2011; Carcaillet et al., 2013; Jomelli et al., 2014), corresponding to the deglacial to Early Holocene events that have been widely reported in higher latitudes (e.g., Briner et al., 2002; Owen et al., 2003; Balco et al., 2009). This study contributes to the growing literature of glacial chronologies in the tropics, strengthening the argument for the broadly synchronous global LGM and deglacial to Early Holocene events between North and South America. In addition, geomorphic evidence, exposure ages, and available radiocarbon dates indicate no glacial events after ~10 ka in either the Morrenas or Talari Valleys. Surface exposure dating of moraines in Venezuela showed similar results, with complete glacial retreat ~9 ka (Carcaillet et al., 2013; Angel et al., 2016) for a study site at a latitude of ~8°48'N, similar to that of our study area in the Cordillera de Talamanca (9°29'N).

Glacial events have been dated to MIS 3 or older in tropical regions of North and South America. In Mexico, the exposure ages of some old moraines have been dated to ~195 ka (Vázquez-Selem and Heine, 2004). In the Andes, moraines have been dated from MIS 4 to as old, or older than, MIS 13 (Farber et al., 2005; Smith et al., 2005, 2008; Kull et al., 2008; Zech et al., 2008; Hein et al., 2009, 2010; Glasser et al., 2011). However, our exposure ages do not indicate the occurrence of glacial events before MIS 2 in our study area of the Cordillera de Talamanca. Postglacial geomorphic processes might have eroded the moraines older than MIS 2, or such moraines may be located below the modern treeline and hidden by dense forest cover, especially on the Caribbean side of the massif. It is also possible that glacial events older than MIS 2 occurred in the Morrenas and Talari Valleys but were less extensive than the LGM event, so that the subsequent LGM advance would have overridden these older moraines. Another possibility is that no glacial events occurred in the highland in Costa Rica prior to the LGM. Further studies are necessary to investigate these different possibilities.

Paleoclimate implications

The global LGM is the coldest period during the last glaciation, and studies indicate considerably more cooling in the tropical highlands than at sea level during this period (Crowley, 2000; Lea, 2004). The ELA depressions of tropical glaciers during the LGM range from 400 to 1400 m (Porter, 2001; Mark et al., 2005) with much higher depressions in the circum-Caribbean highlands (Lachniet and Vazquéz-Selem, 2005). In our study area of the Cordillera de Talamanca, Costa Rica, reconstructed ELA depressions range from 1317 to 1536 m, indicating a cooling of ~7°C to 9°C during the LGM (Orvis and Horn, 2000; Lachniet and Seltzer, 2002; Lachniet and Vazquéz-Selem, 2005). Similarly, reconstructed LGM ELAs were ~850 to 1420 m lower than present in the Cordillera de Mérida, Venezuela, suggesting a temperature depression of 8.8 ± 2°C based on a combined energy and mass-balance equation to account for an ELA lowering (Stansell et al., 2007). Roy and Lachniet (2010) reconstructed ELA depressions during the LGM of 1110 to 1436 m in the Sierra los Cuchumatanes, Guatemala, suggesting a cooling of ~5.9 to 7.6 ± 1.2°C. In contrast, the reconstructions of the sea surface temperatures only indicate 2–3°C depression in the tropics during the LGM (Lee and Slowey, 1999; Lea et al., 2000; Pigati et al., 2008). Several paleotemperature studies from the Cariaco Basin on the north coast of Venezuela indicate a temperature depression of ~3°C to 4°C during the LGM (Lin et al., 1997; Lea et al., 2003).

Various explanations have been proposed to address the discrepancy between the temperature depression reconstructed from the tropical highlands and sea surface during the LGM. One explanation is that the tropical area had a steeper atmospheric lapse rate during the LGM that lowered the freezing height relative to sea surface (Orvis et al, 1997; Farerra et al., 1999; Orvis and Horn, 2000). Betts and Ridgway (1992) suggested other factors, such as a decrease in surface wind speed or an increase in tropical sea surface pressure, may also lower the freezing height. Roy and Lachniet (2010) proposed that the relatively high ELA depressions in Guatemala may be related to the enhanced wetness driven by southward excursions of the boreal winter polar air mass. More studies are needed in the future to address the discrepancy between the temperature depressions reconstructed from low and high altitudes in the tropics.

After the LGM, the temperature presented an overall warming trend to the Early Holocene, but with significant variability (Thompson et al., 1995, 1998). It seems that the Chirripó III–I (M-3, M-2, and M-1) and the T-I moraines in the Morrenas and Talari Valleys were likely formed during short cooling phases from the deglacial period to Early Holocene.

CONCLUSIONS

We constrained glacial chronology in two formerly glaciated valleys in the Chirripó massif of the Cordillera de Talamanca, Costa Rica, using cosmogenic ^{36}Cl surface exposure dating. Forty-nine boulder samples were processed and measured from four moraine complexes in the Morrenas Valley and two moraines in the Talari Valley. The exposure ages of these samples suggest a major glacial event occurred in this area during 25–23 ka, broadly synchronous with the global LGM, followed by periods of retreats and standstills from the deglacial period to the Early Holocene (16–10 ka). The lack of exposure ages of less than ~10 ka is consistent with

https://doi.org/10.1017/qua.2018.133 Published online by Cambridge University Press

evidence from geomorphology and lake sediments that the LGM event and subsequent deglaciation from the deglacial period to the Early Holocene are the most recent glacial events in this area. Cosmogenic exposure ages from these moraines expand the previous glacial chronology determined using radiocarbon ages from basal sediments in glacial lakes and provide important insights into paleoclimate and environmental changes in this tropical highland.

ACKNOWLEDGMENTS

This work was supported by National Science Foundation grant #1227018 to Y. Li and S.P. Horn. Additional support for laboratory analyses and fieldwork was provided by the PRIME Lab (Purdue University), the University of Tennessee, and grants to K.H. Orvis from the American Association of Geographers and to S.P. Horn from the National Geographic Society and the A.W. Mellon Foundation. We thank the Costa Rican Ministry of Environment and Energy and the La Amistad-Pácífico Conservation Area for allowing us to collect samples in Chirripó National Park; Brandon League, Charles Lafon, Carol Harden, and Jose Luis Garita Romero for field assistance; and Maureen Sánchez for logistical assistance. We also thank Chris Fedo, Dakota Anderson, and Yanan Li for laboratory assistance and Marc Caffee, J. Radler, and Tom Clifton for sample preparation and measurement at the PRIME Lab. For constructive comments and suggestions that strengthened the manuscript, we thank Fred Phillips, Lewis Owen, Kathleen Johnson, and an anonymous reviewer.

SUPPLEMENTARY MATERIAL

The supplementary material for this article can be found at https://doi.org/10.1017/qua.2018.133.

REFERENCES

Abramowski, U., Bergau, A., Seebach, D., Zech, R., Glaser, B., Sosin, P., Kubik, P.W., Zech, W., 2006. Pleistocene glaciations of Central Asia: results from ^{10}Be surface exposure ages of erratic boulders from the Pamir (Tajikistan), and the Alay-Turkestan range (Kyrgyzstan). *Quaternary Science Reviews* 25, 1080–1096.

Angel, I., Audemard, F.A., Carcaillet, J., Carrillo, E., Beck, C., Audin, L., 2016. Deglaciation chronology in the Mérida Andes from cosmogenic ^{10}Be dating, (Gavidia valley, Venezuela). *Journal of South American Earth Sciences* 71, 235–247.

Applegate, P.J., Urban, N.M., Keller, K., Lowell, T.V., Laabs, B.J.C., Kelly, M.A., Alley, R.B., 2012. Improving moraine age interpretations through explicit matching of geomorphic process models to cosmogenic nuclide measurements from single landforms. *Quaternary Research* 77, 293–304.

Applegate, P.J., Urban, N.M., Laabs, B.J.C., Keller, K., Alley, R.B., 2010. Modeling the statistical distributions of cosmogenic exposure dates from moraines. *Geoscientific Model Development* 3, 297–307.

Balco, G., 2011. Contributions and unrealized potential contributions of cosmogenic nuclide exposure dating to glacier chronology, 1990-2010. *Quaternary Science Reviews* 30, 3–27.

Balco, G., Briner, J., Finkel, R.C., Rayburn, J.A., Ridge, J.C., Schaefer, J.M., 2009. Regional beryllium-10 production rate calibration for late-glacial northeastern North America. *Quaternary Geochronology* 4, 93–107.

Balco, G., Stone, J.O., Lifton, N., Dunai, T.J., 2008. A complete and easily accessibly means of calculating surface exposure ages or erosion rates from ^{10}Be and ^{26}Al measurements. *Quaternary Geochronology* 3, 174–195.

Barquero, J., Ellenberg, L., 1983. Geomorfologia del Piso Alpino del Chirripó en La Cordillera de Talamanca, Costa Rica. *Revista Geográfica de América Central* 17–18, 293–299.

Barquero, J., Ellenberg, L., 1986. Geomorphologie der alpinen Stufe des Chirripó in Costa Rica. *Eiszeitalter und Gegenwart* 36, 1–9.

Benn, D.I., Owen, L.A., Osmaston, H.A., Seltzer, G.O., Porter, S.C., Mark, B., 2005. Reconstruction of equilibrium-line altitudes for tropical and subtropical glaciers. *Quaternary International* 138–139, 8–21.

Bergoeing, J.P., 1977. Modelado glacier en la Cordillera de Talamanca. *Informe Semestral julio-diciembre 1977*. Instituto Geográfico Nacional, San José, Costa Rica.

Betts, A.K., Ridgway, W., 1992. Tropical boundary layer equilibrium in the last ice age. *Journal of Geophysical Research* 97, 2529–2534.

Borchers, B., Marrero, S.M., Balco, G., Caffee, M., Goehring, B., Lifton, N., Nishiizumi, K., Phillips, F.M., Schaefer, J., Stone, J.O., 2015. Geological calibration of spallation production rates in the CRONUS-Earth project. *Quaternary Geochronology* 31, 188–198.

Briner, J.P., Kaufman, D.S., 2008. Late Pleistocene mountain glaciation in Alaska: key chronologies. *Journal of Quaternary Science* 23, 659–670.

Briner, J.P., Kaufman, D.S., Manley, W.F., Finkel, R.C., Caffee, M.W., 2005. Cosmogenic exposure dating of late Pleistocene moraine stabilization in Alaska. *Geological Society of America Bulletin* 117, 1108–1120.

Briner, J.P., Kaufman, D.S., Werner, A., Caffee, M., Levy, L., Manley, W.F., Kaplan, M.R., Finkel, R.C., 2002. Glacier readvance during the late glacial (Younger Dryas?) in the Ahklun Mountains, southwestern Alaska. *Geology* 30, 679–682.

Bromley, G.R.M., Schaefer, J.M., Winckler, G., Hall, B.L., Todd, C.E., Rademaker, K.M., 2009. Relative timing of last glacial maximum and late-glacial events in the central tropical Andes. *Quaternary Science Reviews* 28, 514–526.

Cane, M.A., 1998. A role for the tropical Pacific. *Science* 282, 59–61.

Carcaillet, J., Angel, I., Carrillo, E., Audemard, F.A., Beck, C., 2013. Timing of the last deglaciation in the Sierra Nevada of the Merida Andes, Venezuela. *Quaternary Research* 80, 482–494.

Castillo-Muñoz, R., 2010. *Glaciaciones e Interglaciaciones en Costa Rica*. Litografía e Imprenta LIL, San José, Costa Rica.

Chen, Y., Li, Y., Wang, Y., Zhang, M., Cui, Z., Yi, C., Liu, G., 2015. Late Quaternary glacial history of the Karlik Range, easternmost Tian Shan, derived from ^{10}Be surface exposure and optically stimulated luminescence datings. *Quaternary Science Reviews* 115, 17–27.

Chiang, J.C.H., 2009. The tropics in paleoclimate. *Annual Review of Earth and Planetary Sciences* 37, 263–297.

Clark, J., McCabe, A.M., Clark, P.U., McCarron, S., Freeman, S.P.H.T., Maden, C., Xu, S., 2009. Cosmogenic ^{10}Be chronology of the last deglaciation of western Ireland, and implications for sensitivity of the Irish Ice Sheet to climate change. *Geological Society of America Bulletin* 121, 3–16.

Crowley, T.J., 2000. CLIMAP SSTs re-revisited. *Climate Dynamics* 16, 241–255.

Denton, G.H., Anderson, R.F., Toggweiler, J.R., Edwards, R.L., Schaefer, J.M., Putnam, A.E., 2010. The last glacial termination. *Science* 328, 1652–1656.

Desilets, D., Zreda, M.G., 2003. Spatial and temporal distribution of secondary cosmic-ray nucleon intensities and applications to in situ cosmogenic dating. *Earth and Planetary Science Letters* 206, 21–42.

Desilets, D., Zreda, M.G., Prabu, T., 2006. Extended scaling factors for in situ cosmogenic nuclides: new measurements at low latitude. *Earth and Planetary Science Letters* 246, 265–276.

Driese, S.G., Orvis, K.H., Horn, S.P., Li, Z., Jennings, D.S., 2007. Paleosol evidence for Quaternary uplift and for climate and ecosystem changes in the Cordillera de Talamanca, Costa Rica. *Palaeogeography, Palaeoclimatology, Palaeoecology* 248, 1–23.

Dunai, T.J., 2000. Scaling factors for production rates of in situ produced cosmogenic nuclides: a critical reevaluation. *Earth and Planetary Science Letters* 176, 157–169.

Dunai, T.J., 2001. Influence of secular variation of the geomagnetic field on production rates of in situ produced cosmogenic nuclides. *Earth and Planetary Science Letters* 193, 197–212.

Dunai, T. J., 2010. *Cosmogenic Nuclides: Principles, Concepts and Applications in the Earth Surface Sciences*. Cambridge University Press, Cambridge.

Farber, D.L., Hancock, G.S., Finkel, R.C., Rodbell, D.T., 2005. The age and extent of tropical alpine glaciation in the Cordillera Blanca, Peru. *Journal of Quaternary Science* 20, 759–776.

Farerra, I., Harrison, S.P., Prentice, I.C., Ramstein, G., Guiot, J., Bartlein, P.J., Bonnefille, R., *et al*., 1999. Tropical climates at the Last Glacial Maximum: a new synthesis of terrestrial palaeoclimate data I. *Vegetation, lake-levels and geochemistry. Climate Dynamics* 15, 823–856.

Gillespie, A., Molnar, P., 1995. Asynchronous maximum advances of mountain and continental glaciers. *Reviews of Geophysics* 33, 311–364.

Glasser, N.F., Clemmens, S., Schnabel, C., Fenton, C.R., McHargue, L., 2009. Tropical glacier fluctuations in the Cordillera Blanca, Peru between 12.5 and 7.6 ka from cosmogenic ^{10}Be Dating. *Quaternary Science Reviews* 28, 3448–3458.

Glasser, N.F., Jansson, K.N., Goodfellow, B.W., Angelis, H., Rodnight, H., Rood, D.H., 2011. Cosmogenic nuclide exposure ages for moraines in the Lago San Martin Valley, Argentina. *Quaternary Research* 75, 636–646.

Gosse, J.C., Phillips, F.M., 2001. Terrestrial in situ cosmogenic nuclides: theory and application. *Quaternary Science Reviews* 20, 1475–1560.

Grubbs, F.E., 1950. Sample criteria for testing outlying observations. *Annals of Mathematical Statistics* 21, 27–58.

Hall, S.R., Farber, D.L., Ramage, J.M., Rodbell, D.T., Finkel, R.C., Smith, J.A., Mark, B.G., Kassel, C., 2009. Geochronology of Quaternary glaciations from the tropical Cordillera Huayhuash, Peru. *Quaternary Science Reviews* 28, 2991–3009.

Hastenrath, S., 1973. On the Pleistocene glaciation of the Cordillera de Talamanca, Costa Rica. *Zeitschrift für Gletscherkunde und Glazialgeologie* 9, 105–121.

Hastenrath, S., 2009. Past glaciation in the tropics. *Quaternary Science Reviews* 29, 790–798.

Hein, A.S., Hulton, N.R.J., Dunai, T.J., Schnabel, C., Kaplan, M.R., Naylor, M., Xu, S., 2009. Middle Pleistocene glaciation in Patagonia dated by cosmogenic-nuclide measurements on outwash gravels. *Earth and Planetary Science Letters* 286, 184–197.

Hein, A.S., Hulton, N.R.J., Dunai, T.J., Sugden, D.E., Kaplan, M.R., Xu, S., 2010. The chronology of the Last Glacial Maximum and deglacial events in central Argentine Patagonia. *Quaternary Science Reviews* 29, 1212–1227.

Herrera, W., 2005. El clima de los páramos de Costa Rica. In: Kappelle, M., Horn, S.P. (Eds.), *Páramos de Costa Rica*. INBIO Press, Santo Domingo, Costa Rica, pp. 113–128.

Heyman, J., Stroeven, A.P., Harbor, J., Caffee, M.W., 2011. Too young or too old: evaluating cosmogenic exposure dating based on an analysis of compiled boulder exposure ages. *Earth and Planetary Science Letters* 302, 71–80.

Horn, S.P., 1990. Timing of deglaciation in the Cordillera de Talamanca, Costa Rica. *Climate Research* 1, 81–83.

Horn, S.P., 1993. Postglacial vegetation and fire history in the Chirripó Páramo of Costa Rica. *Quaternary Research* 40, 107–116.

Horn, S.P., Orvis, K.H., Haberyan, K.A., 2005. Limnology of glacial lakes in the Chirripó Paramo of Costa Rica. In: Kappelle, M., Horn, S.P. (Eds.), *Páramos de Costa Rica*. INBIO Press, Santo Domingo, Costa Rica, pp. 161–181.

Islebe, G.A., Hooghiemstra, H., 1997. Vegetation and climate history of montane Costa Rica since the last glacial. *Quaternary Science Reviews* 16, 589–604.

Jomelli, V., Favier, V., Vuille, M., Braucher, R., Martin, L., Blard, P.-H., Colose, C., *et al*., 2014. A major advance of tropical Andean glaciers during the Antarctic cold reversal. *Nature* 513, 224–228.

Kaplan, M.R., Coronato, A., Hulton, N.R.J., Rabassa, J.O., Kubik, P.W., Freeman, S.P.H.T., 2007. Cosmogenic nuclide measurements in southernmost South America and implications for landscape change. *Geomorphology* 87, 284–301.

Kaplan, M.R., Fogwill, C.J., Sugden, D.E., Hulton, N.R.J., Kubik, P.W., Freeman, S.P.H.T., 2008. Southern Patagonia glacial chronology for the Last Glacial period and implications for Southern Ocean climate. *Quaternary Science Reviews* 27, 284–294.

Kaplan, M.R., Strelin, J.A., Schaefer, J.M., Denton, G.H., Finkel, R.C., Schwartz, R., Putnam, A.E., Vandergoes, M.J., Goehring, B.M., Travis, S.G., 2011. In-situ cosmogenic ^{10}Be production rate at Lago Argentino, Patagonia: implications for late-glacial climate chronology. *Earth and Planetary Science Letters* 309, 21–32.

Kappelle, M., Horn, S.P., 2005. *Páramos de Costa Rica*. INBIO Press, Santo Domingo, Costa Rica.

Kappelle, M., Horn, S.P., 2016. The *Páramo* ecosystem of Costa Rica's highlands. In: Kappelle, M. (Ed.), *Costa Rican Ecosystems*. University of Chicago Press, Chicago, pp. 492–523.

Kaser, G., Osmaston, H., 2002. *Tropical Glaciers*. Cambridge University Press, Cambridge.

Koppes, M., Gillespie, A.R., Burke, R.M., Thompson, S.C., Stone, J., 2008. Late Quaternary glaciation in the Kyrgyz Tien Shan. *Quaternary Science Reviews* 27, 846–866.

Kull, C., Imhof, S., Grosjean, M., Zech, R., Veit, H., 2008. Late Pleistocene glaciation in the Central Andes: temperature versus humidity control – a case study from the eastern Bolivian Andes (17°S) and regional synthesis. *Global and Planetary Change* 60, 148–164.

Laabs, B.J.C., Munroe, J.S., Best, L.C., Caffee, M.W., 2013. Timing of the last glaciation and subsequent deglaciation in the Ruby Mountains, Great Basin, USA. *Earth and Planetary Science Letters* 361, 16–25.

Lachniet, M.S., 2004. Quaternary glaciation in Guatemala and Costa Rica. In: Ehlers, J., Gibbard, P.L. (Eds.), *Quaternary*

https://doi.org/10.1017/qua.2018.133 Published online by Cambridge University Press

Glaciations – Extent and Chronology. Part III: South America, Asia, Africa, Australasia, Antarctica. Developments in Quaternary Science, Vol. 2, Part C. Elsevier, Amsterdam, pp. 135–138.

Lachniet, M.S., 2007. Glacial geology and geomorphology. In: Bundschuh, J., Alvarado, G.E. (Eds.), *Central America: Geology, Resources, and Hazards*. Vol. 1. Taylor and Francis/Balkema, Leiden, the Netherlands, pp. 171–184.

Lachniet, M.S., Roy, A.J., 2011. Costa Rica and Guatemala. In Ehlers, J., Gibbard, P.L., Hughes, P.D. (Eds.), *Quaternary Glaciations – Extent and Chronology: A Closer Look*. Developments in Quaternary Science 15. Elsevier, Amsterdam, the Netherlands, pp. 843–848.

Lachniet, M.S., Seltzer, G.O., 2002. Late Quaternary glaciation of Costa Rica. *Geological Society of America Bulletin* 114, 547–558.

Lachniet, M.S., Vázquez-Selem, L., 2005. Last glacial maximum equilibrium line altitudes in the CircumCaribbean (Mexico, Guatemala, Costa Rica, Colombia, and Venezuela). *Quaternary International* 138–139, 129–144.

Lal, D., 1991. Cosmic ray labeling of erosion surfaces: in situ nuclide production rates and erosion models. *Earth and Planetary Science Letters* 104, 424–439.

Lane, C.S., Horn, S.P., 2013. Terrestrially-derived *n*-alkane δD evidence of shifting Holocene paleohydrology in highland Costa Rica. *Arctic, Antarctic, and Alpine Research* 45, 342–349.

Lane, C.S., Horn, S.P., Mora, C.L., Orvis, K.H., Finkelstein, D.B., 2011. Sedimentary stable carbon isotope evidence of late Quaternary vegetation and climate change in highland Costa Rica. *Journal of Paleolimnology* 45, 323–338.

Lea, D.W., 2004. The 100 000-yr cycle in tropical SST, greenhouse forcing, and climate sensitivity. *Journal of Climate* 17, 2170–2179.

Lea, D.W., Pak, D.K., Peterson, L.C., Hughen, K.A., 2003. Synchronicity of tropical and high-latitude Atlantic temperatures over the last glacial termination. *Science* 301, 1361–1364.

Lea, D.W., Pak, D.K., Spero, H.J., 2000. Climate impact of late Quaternary equatorial Pacific sea surface temperature variations. *Science* 289, 1719–1724.

Lee, K.E., Slowey, N.C., 1999. Cool surface waters of the subtropical North Pacific Ocean during the last glacial. *Nature* 397, 512–514.

Li, Y., 2013. Determining topographic shielding from digital elevation models for cosmogenic nuclide analysis: a GIS approach and field validation. *Journal of Mountain Science* 10, 355–362.

Li, Y., Harbor, J., 2009. Cosmogenic nuclides and geomorphology: theory, limitations and applications. In: Ferrari, D.M., Guiseppie, A.R. (Eds.), *Geomorphology and Tectonics*. Nova Science, Hauppauge, New York, pp. 1–33.

Li, Y., Liu, G., Chen, Y., Li, Y., Harbor, J., Stroeven, A.P., Caffee, M., Zhang, M., Li, C., Cui, Z., 2014. Timing and extent of Quaternary glaciations in the Tianger Range, eastern Tian Shan, China, investigated using ^{10}Be surface exposure dating. *Quaternary Science Reviews* 98, 7–23.

Li, Y., Liu, G., Kong, P., Harbor, J., Chen, Y., Caffee, M., 2011. Cosmogenic nuclide constraints on glacial chronology in the source area of the Urumqi River, Tian Shan, China. *Journal of Quaternary Science* 26, 297–304.

Licciardi, J.M., Pierce, K.L., 2008. Cosmogenic exposure-age chronologies of Pinedale and Bull Lake glaciations in greater Yellowstone and the Teton Range, USA. *Quaternary Science Reviews* 27, 814–831.

Licciardi, J.M., Schaefer, J.M., Taffart, J.R., Lund, D.C., 2009. Holocene glacier fluctuations in the Peruvian Andes indicate northern climate linkages. *Science* 325, 1677–1679.

Lifton, N., Sato, T., Dunai, T.J., 2014. Scaling in situ cosmogenic nuclide production rates using analytical approximations to atmospheric cosmic-ray fluxes. *Earth and Planetary Science Letters* 386, 149–160.

Lifton, N., Smart, D.F., Shea, M.A., 2008. Scaling time-integrated in situ cosmogenic nuclide production rates using a continuous geomagnetic model. *Earth and Planetary Science Letters* 268, 190–201.

Lifton, N.A., Bieber, J.W., Clem, J.M., Duldig, M.L., Evenson, P., Humble, J.E., Pyle, R., 2005. Addressing solar modulation and long-term uncertainties in scaling in situ cosmogenic nuclide production rates. *Earth and Planetary Science Letters* 239, 140–161.

Lin, H.L., Peterson, L.C., Overpeck, J.T., Trumbore, S.E., Murray, D.W., 1997. Late Quaternary climate change from δ^{18}O records of multiple species of planktonic foraminifera: high-resolution records from the anoxic Cariaco Basin, Venezuela. *Paleoceanography* 12, 415–427.

Mark, B.G., Harrison, S.P., Spessa, A., New, M., Evans, D.J.A., Helmens, K.F., 2005. Tropical snowline changes at the last glacial maximum: a global assessment. *Quaternary International* 138–139, 168–201.

Marrero, S.M., Phillips, F.M., Borchers, B., Lifton, N., Aumer, R., Balco, G., 2016a. Cosmogenic nuclide systematics and the CRONUScalc program. *Quaternary Geochronology* 31, 160-187.

Marrero, S.M., Phillips, F.M., Caffee, M.W., Gosse, J.G., 2016b. CRONUS-Earth cosmogenic ^{36}Cl calibration. *Quaternary Geochronology* 31, 199–219.

Martin, P.S., 1964. Paleoclimatology and a tropical pollen profile. Report of the VIth International Congress on the Quaternary, Warsaw, 1961. Vol. 2. *INQUA*, Łódź, Poland, pp. 319–323.

Nishiizumi, K., Winterer, E.L., Kohl, C.P., Klein, J., Middleton, R., Lal, D., Arnold, J.R., 1989. Cosmic ray production rates of ^{10}Be and ^{26}Al in quartz from glacially polished rocks. *Journal of Geophysical Research* 94, 17907–17915.

Orvis, K.H., Clark, G.M., Horn, S.P., Kennedy, L.M., 1997. Geomorphic traces of Quaternary climates in the Cordillera Central, Dominican Republic. *Mountain Research and Development* 17, 323–331.

Orvis, K.H., Horn, S.P., 2000. Quaternary glaciers and climate on Cerro Chirripó, Costa Rica. *Quaternary Research* 54, 24–37.

Owen, L.A., Finkel, R.C., Minnich, R.A., Perez, A.E., 2003. Extreme southwestern margin of late Quaternary glaciation in North America: timing and controls. *Geology* 31, 729–732.

Phillips, F.M., Stone, W.D., Fabryka-Martin, J.T., 2001. An improved approach to calculating low-energy cosmic ray neutron fluxes near the land/atmosphere interface. *Chemical Geology* 175, 689–701.

Phillips, F.M., Zreda, M., Plummer, M.A., Elmore, D., Clark, D.H., 2009. Glacial geology and chronology of Bishop Creek and vicinity, eastern Sierra Nevada, California. *Geological Society of America Bulletin* 121, 1013–1033.

Pigati, J.S., Zreda, M., Zweck, C., Almasi, P.F., Elmore, D., Sharp, W.D., 2008. Ages and inferred causes of late Pleistocene glaciations on Mauna Kea, Hawai'i. *Journal of Quaternary Science* 23, 683–702.

Porter, S.C., 2001. Snowline depression in the tropics during the last glaciation. *Quaternary Science Reviews* 20, 1067–1091.

Putnam, A.E., Schaefer, J.M., Denton, G.H., Barrell, D.J.A., Birkel, S.A., Andersen, B.G., Kaplan, M.R., Finkel, R.C.,

https://doi.org/10.1017/qua.2018.133 Published online by Cambridge University Press

Schwartz, R., Doughty, A.M., 2013. The Last Glacial Maximum at 44°S documented by a moraine chronology at Lake Ohau, Southern Alps of New Zealand. *Quaternary Science Reviews* 62, 114–141.

Reimer, P.J., Bard, E., Bayliss, A., Beck, J.W., Blackwell, P.G., Ramsey, C.B., Buck, C.E., *et al*., 2013. IntCal13 and Marine13 Radiocarbon age calibration curves 0–50,000 years cal BP. *Radiocarbon* 55, 1869–1887.

Rippington, S., Cunningham, D., England, R., 2008. Structure and petrology of the Altan Uul ophiolite: new evidence for a Late Carboniferous suture in the Gobi Altai, southern Mongolia. *Journal of the Geological Society* 165, 711–723.

Rood, D.H., Burbank, D.W., Finkel, R.C., 2011. Chronology of glaciations in the Sierra Nevada, California, from ^{10}Be surface exposure dating. *Quaternary Science Reviews* 30, 646–661.

Roy, A.J., Lachniet, M.S., 2010. Late Quaternary glaciation and equilibrium-line altitudes of the Maya Ice Cap, Guatemala, Central America. *Quaternary Research* 74, 1–7.

Schaefer, J.M., Denton, G.H., Barrell, D.J.A., Ivy-Ochs, S., Kubik, P.W., Andersen, B.G., Phillips, F.M., Lowell, T.M., Schluchter, C., 2006. Near-synchronous interhemispheric termination of the Last Glacial Maximum in mid-latitudes. *Science* 312, 1510–1513.

Schaefer, J., Denton, G., Kaplan, M., Putnam, A., Finkel, R., Barrell, D., Andersen, B., *et al*., 2009. High-frequency Holocene glacier fluctuations in New Zealand differ from the northern signature. *Science* 324, 622–625.

Schimmelpfennig, I., Benedetti, L., Finkel, R., Pik, R., Blard, P.H., Bourlès, D., Burnard, P., Williams, A., 2009. Sources of in-situ ^{36}Cl in basaltic rocks. Implications for calibration of production rates. *Quaternary Geochronology* 4, 441–461.

Seltzer, G.O., 2001. Late Quaternary glaciation in the tropics: future research directions. *Quaternary Science Reviews* 20, 1063–1066.

Smith, C.A., Lowell, T.V., Caffee, M.W., 2009. Lateglacial and Holocene cosmogenic surface exposure age glacial chronology and geomorphological evidence for the presence of cold-based glaciers at Nevado Sajama, Bolivia. *Journal of Quaternary Science* 24, 360–372.

Smith, C.A., Lowell, T.V., Owen, L.A., Caffee, M.W., 2011. Late Quaternary glacial chronology on Nevado Illimani, Bolivia, and the implications for paleoclimatic reconstructions across the Andes. *Quaternary Research* 75, 1–10.

Smith, J.A., Mark, B.G., Rodbell, D.T., 2008. The timing and magnitude of mountain glaciation in the tropical Andes. *Journal of Quaternary Science* 23, 609–634.

Smith, J.A., Rodbell, D.T., 2010. Cross-cutting moraines reveal evidence for North Atlantic influence on glaciers in the tropical Andes. *Journal of Quaternary Science* 25, 243–248.

Smith, J.A., Seltzer, G.O., Farber, D.L., Rodbell, D.T., Finkel, R.C., 2005. Early local last glacial maximum in the tropical Andes. *Science* 308, 678–681.

Stansell, N.D., Polissar, P.J., Abbott, M.B., 2007. Last glacial maximum equilibrium-line altitude and paleo-temperature reconstructions for the Cordillera de Mérida, Venezuelan Andes. *Quaternary Research* 67, 115–127.

Stone, J., 2000. Air pressure and cosmogenic isotope production. *Journal of Geophysical Research* 105, 23753–23760.

Stuiver, M., Reimer, P.J., 1993. Extended ^{14}C database and revised CALIB radiocarbon calibration program. *Radiocarbon* 35, 215–230.

Swanson, T.W., Caffee, M., 2001. Determination of ^{36}Cl production rates derived from the well-dated deglaciation surfaces of Whidbey and Fidalgo Islands, Washington. *Quaternary Research* 56, 366–382.

Thompson, L.G., Davis, M.E., Thompson, E.M., Sowers, T.A., Henderson, K.A., Zagorodnov, V.S., Lin, P.N., *et al*., 1998. A 25,000 year tropical climate history from Bolivian ice cores. *Science* 282, 1858–1864.

Thompson, L.G., Mosley-Thompson, E., Davis, M.E., Lin, P-N., Henderson, K.A., Cole-Dai, J., Bolzan, J.F., Liu, K-B., 1995. Late glacial stage and Holocene tropical ice core records from Huscarán, Peru. *Science* 269, 46–50.

Vázquez-Selem, L., Heine, K., 2004. Late Quaternary glaciation in Mexico. In: Ehlers, J., Gibbard, P.L. (Eds.), *Quaternary Glaciations – Extent and Chronology*. Part III: South America, Asia, Africa, Australasia, Antarctica. Developments in Quaternary Science, Vol. 2, Part C. Elsevier, Amsterdam, pp. 233–242.

Wesnousky, S.G., Aranguren, R., Rengifo, M., Owen, L.A., Caffee, M.W., Murari, M.K., Perez, O.J., 2012. Toward quantifying geomorphic rates of crustal displacement, landscape development, and the age of glaciation in the Venezuelan Andes. *Geomorphology* 141–142, 99–113.

Weyl, R., 1956a. Eiszeitliche gletscherspuren in Costa Rica (Mittelamerika). *Zeitschrift für Gletscherkunde und Glazialgeologie* 3, 317–325.

Weyl, R., 1956b. Spuren eiszeitlicher vergletscherung in der Cordillera de Talamanca Costa Rica (Mittelamerika). *Neues Jahrbuch für Geologie und Palaontologie* 102, 283–294.

Wunsch, O., Calvo, G., Willscher, B., Seyfried, H., 1999. Geologie der alpinen Zone des Chirripó-Massives (Cordillera de Talamanca, Costa Rica, Mittelamerika). *Profil* 16, 193–210.

Young, N.E., Briner, J.P., Kaufman, D.S., 2009. Late Pleistocene and Holocene glaciation of the Fish Lake valley, northeastern Alaska Range, Alaska. *Journal of Quaternary Science* 24, 677–689.

Young, N.E., Briner, J.P., Leonard, E.M., Licciardi, J.M., Lee, K., 2011. Addressing climatic and nonclimatic forcing of Pinedale glaciation and deglaciation in the western United States. *Geology* 39, 171–174.

Zech, R., Kull, C., Veit, H., 2006. Late Quaternary glacial history in the Encierro Valley, northern Chile (29°S), deduced from ^{10}Be surface exposure dating. *Palaeogeography, Palaeoclimatology, Palaeoecology* 234, 277–286.

Zech, R., May, J.-H., Kull, C., Ilgner, J., Kubik, P.W., Veit, H., 2008. Timing of the late Quaternary glaciation in the Andes from ~15 to 40° S. *Journal of Quaternary Science* 23, 635–647.

Zech, J., Zech, R., Kubik, P.W., Veit, H., 2009. Glacier and climate reconstruction at Tres Lagunas, NW Argentina, based on ^{10}Be surface exposure dating and lake sediment analyses. *Palaeogeography, Palaeoclimatology, Palaeoecology* 284, 180–190.

https://doi.org/10.1017/qua.2018.133 Published online by Cambridge University Press